



Terrestrial and marine dynamics on the brink of the Messinian salinity crisis: A wet scenario from the northern Mediterranean

Adele Bertini^{a,*}, Gabriele Niccolini^a, Rocco Gennari^b, Francesca Lozar^b, Elena Menichetti^a, Marcello Natalicchio^b, Francesco Dela Pierre^b

^a Dipartimento di Scienze della Terra, Università degli Studi di Firenze, Via G. la Pira 4, Firenze 50121, Italy

^b Dipartimento di Scienze della Terra, Università degli Studi di Torino, Via Valperga Caluso 35, Torino 10125, Italy

ARTICLE INFO

Editor: Dr. Fabienne Marret-Davies

Keywords:

Pollen
Organic-walled dinoflagellate cysts
Calcareous plankton
Paleoclimate
Late Miocene
Piedmont basin

ABSTRACT

The ongoing debate on the causes and modalities of the Messinian Salinity Crisis (MSC) from 5.971 Ma needs to be implemented by an in-depth knowledge of the events and changes, on a global to regional scale, that have preceded its onset. Here we use palynological (pollen and dinocysts) and micropaleontological (foraminifers and calcareous nannoplankton) quantitative analyses from the Govone sedimentary succession (Northern Italy, western Mediterranean) to reconstruct the cyclical changes in atmosphere, surface, and deep-water hydrographic conditions during the Late Miocene, prior to the onset of the MSC (from ca 6.6 Ma) and across it (up to 5.96 Ma). On land, plant communities were dominated by arboreal life forms typical of warm and humid conditions. However, mid- to high altitude coniferous taxa attest to a sequence of cold to cool conditions, some coinciding with glacial obliquity-controlled phases, notably those across the MSC onset (i.e. TG34 and TG32). Dominant trees were Taxodiaceae, especially in freshwater swamps, during warm and humid phases. The latter alternate with relatively less warm, and less humid phases characterised by the reduction of Taxodiaceae, according to the precession-controlled sedimentary cyclicity (sapropel-marl couplets). The absence of any significant expansion in the herbaceous cover is evidence of no substantial increases in aridity at insolation minima. In the marine realm, the precession-controlled cycles correspond to prevalent alternations between warm water, oligotrophic (sapropel, insolation maxima) and cool water, eutrophic (marls, insolation minima) conditions. The progressive decrease of oceanic/outer neritic dinocyst taxa, along with a more continuous occurrence of the inner neritic ones, confirm the progressive restriction of Mediterranean and Atlantic connections, despite oceanic influxes, the latest at 6.14 Ma and 6.05 Ma. On the other hand, the occurrence of freshwater episodes, according to dinocysts, does not exclude possible connections with Paratethys, at 6.18 Ma and 6.07 Ma. All calcareous nannoplankton and foraminifera apparently disappear from the sedimentary record before the onset of the MSC, at ca 6.02 Ma; however, dinocysts allow the documentation of the history of pre-evaporitic conditions up to the beginning of the MSC onset, when lagoons, marked by frequent salinity changes, expanded in the inner neritic zone of the Govone intermediate depth basin, during ca 60 kyrs. Plant assemblages attest a long-lasting increase of seasonality (from 6.2 Ma) as well as a peculiar inversion in the dominant vegetal patterns of the sapropel-marl couplets, between ca 6.02 Ma and 5.96 Ma, corresponding to the uppermost four cycles. The significant restriction of the marine environment, after 6.02 Ma, possibly promoted atmospheric changes marked by reduced vs enhanced activity of the Mediterranean storm-track in phase with precession. This, in turn, regulated the amounts of runoff in the Northern Italian sectors from the Alps.

1. Introduction

Since the late Neogene, Mediterranean environments and ecosystems have undergone substantial transformations, influenced by two major

and noteworthy changes, within a paleogeographic context increasingly resembling the present one. They are the Messinian Salinity Crisis (MSC, 5.97–5.33 Ma) and the expansion of Arctic ice with the Quaternary Glacial/Interglacial cycles onset (from about 2.6 Ma), acting at regional

* Corresponding author.

E-mail addresses: adele.bertini@unifi.it (A. Bertini), rocco.gennari@unito.it (R. Gennari), francesca.lozar@unito.it (F. Lozar), marcello.natalicchio@unito.it (M. Natalicchio), francesco.delapierre@unito.it (F. Dela Pierre).

<https://doi.org/10.1016/j.gloplacha.2024.104362>

Received 21 July 2023; Received in revised form 26 December 2023; Accepted 12 January 2024

Available online 18 January 2024

0921-8181/© 2024 The Authors. Published by Elsevier B.V. This is an open access article under the CC BY-NC-ND license (<http://creativecommons.org/licenses/by-nc-nd/4.0/>).

and global scale, respectively (e.g. Shackleton et al., 1984; Berger and Loutre, 2010; Roveri et al., 2014). The late Neogene includes the terminal part of the gradual trends of warming and cooling driven by tectonic processes on time scales of 10^5 to 10^7 years, since 65 Ma (Zachos et al., 2001). A dominant cooling trend, especially developed after ca 13.9 Ma, marked the transition from the cool- to the icehouse, after 3.3 Ma (Westerhold et al., 2020). Between 5.97 Ma and 5.33 Ma tectonics also played a key role in the history of Mediterranean-Atlantic connections (open vs closed) promoting both the onset of the MSC, marked by the isolation of the Mediterranean basin and the development of hyper-saline conditions, and its end, ca 640 kyr later when the connection was re-established (e.g. Capella et al., 2019, 2020 and references therein). Climate, superimposed on the longer-term tectonic trend, was also active by the dominant precession controlled regional climate changes plus a dominantly obliquity related glacial cyclicality (e.g. Hilgen and Krijgsman, 1999; Krijgsman et al., 2001; Sierro et al., 2001).

Broad-leaved evergreen-warm mixed forest and xerophytic woods-scrub/warm grass-shrub biomes largely characterised the northern and southern late Neogene Mediterranean terrestrial landscapes, respectively (e.g. Fauquette et al., 1999, 2006; Bertini, 2006; Jiménez-Moreno et al., 2010; Jiménez-Moreno et al., 2013). Mediterranean-type taxa, already present since the Paleocene, were sporadic at that time, increasing in importance solely during the last several thousand years of the Quaternary, as documented by pollen records (e.g. Combourieu-Nebout et al., 2015; Bertini and Combourieu-Nebout, 2023). Nowadays the Mediterranean vegetation is, on the contrary, largely expanded in the Mediterranean Region (MR), especially along its littoral, under a prevalent Mediterranean climate typified by long dry summers and mild-wet winters. However, the increasing effects of the Global Warming are producing rising temperatures and changes in both the distribution and intensity of precipitation. Recent climate models also identify the MR as a hot spot of climate change (e.g. Giorgi, 2006; Lionello et al., 2006; Lionello et al., 2012; Lionello et al., 2023; Christensen et al., 2007; Giorgi and Lionello, 2008; Planton et al., 2012; Collins et al., 2013; Gualdi et al., 2013; Ulbrich et al., 2013; Lionello and Scarascia, 2018, 2020; Cos et al., 2022). Namely, the MR is warming at a higher rate than the global annual mean surface temperature, with values particularly significant in summer and in the continental areas, north of the basin. A significant reduction in precipitation is also expected which is in contrast with the general increase of the hydrological cycle. In such

a context, the consequences of a reduction of Atlantic-Mediterranean connections, could be dramatic, nowadays. The geological records documenting the times and modality of transition from pre-evaporitic to evaporitic conditions as well as the parallel responses of the marine and terrestrial ecosystems can provide insights that could help predicting the effects of the current climate change. For this reason, it is crucial to explain how we get to the beginning of the crisis, and what impact the interruption of Atlantic-Mediterranean connections had on biological communities in both marine and terrestrial realms (e.g. Bahr et al., 2022).

The Piedmont basin (Govone site; Fig. 1) represents a key area, in the Mediterranean, for understanding the main paleoceanographic and atmospheric circulation changes during this critical period of the Late Miocene history. Here, the stratigraphically continuous transition between pre-evaporitic open marine deposits and the first evaporites at 5.97 Ma (Dela Pierre et al., 2011) is typified by a distinct lithological cyclicality which was associated to astronomical-induced climatic variations (Gennari et al., 2020; Sabino et al., 2020). Micropaleontological data (pollen, dinocysts, foraminifers and calcareous nannoplankton) provide a substantial improvement of the Late Miocene geological database and allow us to better understand the complex mechanisms that led to the onset of the MSC.

2. Latest Neogene paleoenvironments and paleoclimate in the Mediterranean

The Mediterranean Sea is bounded, almost entirely, by emerged land, at least since the Tortonian. The corridor connecting the Eastern Mediterranean Sea to the Indian ocean was already closed since the Serravallian, in response of a global sea level fall linked to the onset of permanent glaciation on the Antarctic continent (Bialik et al., 2019 and references therein) and the northward migration of the African and Arabian plates (Hüsing et al., 2009). The Late Miocene tectonic activity also induced important changes in the land mass distribution, in the gateway areas and in the peri-Mediterranean chains (e.g. the emersion of the Apennines and other mountain ranges such as the Betic Cordillera; Mather et al., 2001; Artoni et al., 2004; Carminati and Doglioni, 2012; Krijgsman et al., 2018). The connection with the Atlantic Ocean to the West was open through the Betic and Rifian corridors up to the early Messinian (age of the uppermost marine sediments in the Rifian area, Capella et al., 2018) and later through the proto-Gibraltar strait



Fig. 1. Location of the Govone section (Piedmont basin, Italy) and of the main sites cited in the text.

(Krijgsman et al., 2018 and references therein). The role of eustatic versus tectonic control as well as the main paleoceanographic events in the Rifian Strait area, before, during and just after the MSC, were also documented by palynological studies in the late Neogene Salé core (Atlantic coast of northern Morocco, near Bou Regreg) (Warny and Wrenn, 2002; Warny et al., 2003). Intermittent connections with the Paratethys also occurred to the East (Stoica et al., 2013; Krijgsman et al., 2020 and references therein) (Fig. 2). This important paleogeographic reorganization was accompanied by major changes of the atmospheric circulation during an overall cooling trend, starting from the Middle Miocene (permanent Eastern Antarctic ice sheet, Shevenell et al., 2008; Holbourn et al., 2013). An acceleration of the cooling trend driven by a pCO_{2atm} drop (Tortonian/Messinian) and the onset of (transient) Northern Hemisphere glaciations (at ca 6.3–6.2 Ma; Herbert et al., 2016; Holbourn et al., 2018) or earlier (Larsen et al., 1994) is also evident during the Late Miocene (Fig. 2). Besides the similar paleogeography, it is assumed that the Late Miocene Mediterranean circulation was similar to the modern thermohaline pattern and that an anti-estuarine circulation was established at the Atlantic gateways (e.g. Kouwenhoven and van der Zwaan, 2006). However, hydrographic models based on the $^{87}Sr/^{86}Sr$ isotope ratio and climatic simulations suggest that, during the Messinian, runoff from North African rivers was strongly enhanced with respect to the modern configuration (Gladstone et al., 2007; Simon et al., 2017), causing important alterations of the thermohaline circulation in the Mediterranean (Fig. 2). An additional runoff source was identified in the Chad and Eosahabi basins (Central Africa), contributing to the relatively more positive hydrological budget at time of 65°N summer insolation maxima, when runoff was stronger. According to climatic simulation (Simon et al., 2017), such extra freshwater budget would

have prevented phase-offset between sapropel formation and insolation maxima, especially during three intervals: base and top of the Messinian and at around 6.1–6.0 Ma, when the freshwater budget shows an opposite phase relation with insolation (Fig. 2).

2.1. The late Tortonian-Messinian sedimentation in the Mediterranean before the MSC onset

During the Neogene the most remarkable feature of marine Mediterranean sedimentary successions is the strikingly regular superimposition of lithological cycles (e.g. Hilgen and Krijgsman, 1999; Krijgsman et al., 2004) composed of laminated shales/sapropels (hereafter termed sapropels) and marls/carbonates, with intercalated diatomites during the Messinian pre-evaporitic phase. These lithological cycles were described in several sedimentary sections (Fig. 2) and their genesis and significance discussed in many papers, especially for the interval spanning from the Tortonian/Messinian boundary to the MSC onset (e.g. Hilgen et al., 1995; Hilgen and Krijgsman, 1999; Sierró et al., 2001; Blanc-Valleron et al., 2002; Krijgsman et al., 2004; Kouwenhoven et al., 2006; Rouchy and Caruso, 2006; Drinia et al., 2007; Manzi et al., 2007, 2011, 2016; Pellegrino et al., 2018; Natalicchio et al., 2019; Gennari et al., 2020; Mancini et al., 2020; Sabino et al., 2020). The regular accumulation of dark organic-rich layers (sapropels) since the Middle Miocene is a peculiarity of the Mediterranean basin (e.g. Nijenhuis et al., 1996); before and after the Messinian their formation is limited to periods of insolation maxima and high eccentricity (Hilgen et al., 1995, 2003; Schenau et al., 1999). Their origin is linked to the increase of runoff at time of 65°N summer insolation maxima and the consequent increase in productivity and stratification of the water column (Rohling

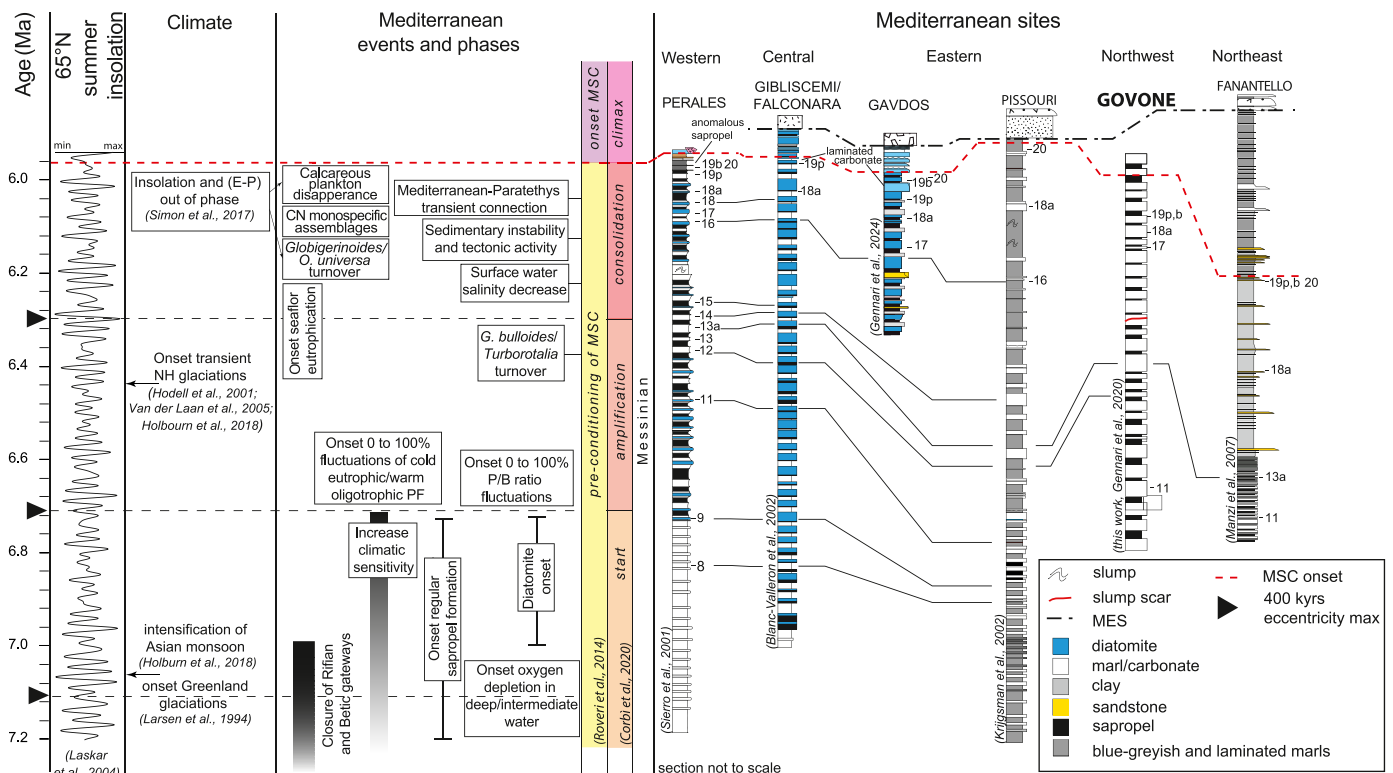


Fig. 2. Selected Mediterranean sites and main late Tortonian-Messinian events. Calcareous Nannoplankton (CN), Eccentricity-Precession (E-P), Messinian Erosional Surface (MES), Messinian Salinity Crisis (MSC), Northern Hemisphere (NH), Plankton/Benthos (P/B), Planktic Foraminifers (PF). Numbers represent bioevents as labelled and described in the text (event numeration modified from Sierró et al., 2001 and Gennari et al., 2018): 7 is the bottom acme of *G. nicolae*; 8 is the top acme of *G. nicolae*; 11 is the last regular occurrence of *G. miotumida* gr.; 12 is the first abundant occurrence of *T. multiloba*; 13 is the last regular influx of left coiled Neogloboquadrinids; 13a is the cooling change from left to right coiled Neogloboquadrinids; 14 is the first abundant influx of right coiled Neogloboquadrinids; 15 is the first influx of *Globorotalia scitula*; 16 is the influx of left coiled Neogloboquadrinids; 17 is the second influx of *G. scitula*; 18a is the last occurrence of *T. multiloba*; 19p is the last recovery of planktic foraminifera and 19b is the last recovery of benthic foraminifera; 20 is the CN MSC onset bioevent of Lozar and Negri (2019) and Mancini et al. (2020). (Gennari et al., 2024; Krijgsman et al., 2002).

et al., 2015). Instead, starting from 7.16 Ma (at Falconara, Figs. 1, 2) or 6.7 Ma (at Perales, Figs. 1, 2), sapropels formed also during less pronounced insolation maxima, at time of eccentricity minima (Hilgen et al., 1995). The increased regularity of sapropels formation is attributed to the restricted Mediterranean circulation originated by the tectonic reorganization of the Atlantic gateways (e.g. Krijgsman et al., 2018), which enhanced the sensitivity of the Mediterranean oceanography to orbitally-controlled climatic changes. The quantification of the Mediterranean freshwater budget also includes an extra African runoff source to explain the regular sapropels formation before the MSC (Simon et al., 2017), as stated above. The enhanced climatic sensitivity also resulted in another distinctive feature of the Messinian cycles: the occurrence of diatomaceous intervals. In fact, moving from maxima to minima in insolation, diatomites formed in several Mediterranean sections (Perales, Falconara, Gavdos, among others; Figs. 1, 2) during periods of enhanced siliceous productivity and silica preservation (Pellegrino et al., 2018 and references therein). Diatomite deposition was favoured by increasing availability of dissolved silica from the continent, both by means of runoff and aeolian transport during a period of open habitats expansion (Pellegrino et al., 2018), and from a well-mixed water column. However, in the Northern Mediterranean, diatomites have only a scattered, local occurrence (Pecetto di Valenza, Piedmont basin; Pellegrino et al., 2020a, 2020b), but they are apparently absent in other sections of the Piedmont basin (Pollenzo and Govone; Dela Pierre et al., 2011, 2012; Lozar et al., 2018; Gennari et al., 2020), in the Vena del Gesso basin (Monte del Casino and Monticino sections; Krijgsman et al., 1999; Kouwenhoven et al., 2003) and in the Northern Apennine foredeep (Fananello borehole, Sapigno basin; and Legnagnone section; Manzi et al., 2007; Gennari et al., 2013) (Figs. 1, 2).

2.2. The chronology of the main events in the marine realm

The use of stratigraphic tools to recognize the strong imprint of the insolation on the pre-evaporitic sedimentary successions across the Mediterranean allowed a bed-by-bed correlation among sections located thousands of km apart (e.g. Krijgsman et al., 1999; Raffi et al., 2003; Sierro et al., 2003; Krijgsman et al., 2004). Biostratigraphy, magnetostratigraphy and radiometric dating were used in support of cyclostratigraphy to build the stratigraphic framework of the pre-evaporitic Mediterranean successions and to describe the similar and synchronous history of the progressive restriction of the Mediterranean towards the MSC onset (Blanc-Valleron et al., 2002; Filippelli et al., 2003; Corbí et al., 2020; Gennari et al., 2020 and references therein). Successive steps, roughly coinciding with 400 kyr eccentricity maxima (Fig. 2; Kouwenhoven et al., 2006) are clearly recognizable in the micropaleontological record and imply important changes in the paleoceanography of the Mediterranean. Following Kouwenhoven et al. (2006), Corbí et al. (2020) introduced a new terminology to identify the following phases of the restriction: start, amplification, consolidation (Fig. 2). They correspond to the “pre-conditioning phase of the MSC” of Roveri et al. (2014). Moreover, the expression “climax of the restriction” was introduced for the last phase of the Mediterranean restriction, which corresponds to the MSC onset at 5.97 Ma (Manzi et al., 2013). The “start phase” (sensu Corbí et al., 2020) begins at 7.16 Ma, when restricted marine conditions are first and widely attested by the onset of regular sapropel accumulation in deeper succession (e.g. Metochia and Gibliscemi/Falconara sections; Figs. 1, 2) at time of insolation maxima. The same mechanism also caused the disappearance of oxyphilic benthic foraminifera (BF) (Kouwenhoven et al., 2006). The oxygen depletion at the seafloor progressively invaded the shelf region (e.g., the Sorbas basin, Western Mediterranean; Sierro et al., 2001) where sapropels only deposited from 6.7 Ma; however, in shallower sections, like Legnagnone (Fig. 1; North-eastern Apennine; Gennari et al., 2013) the seafloor was less affected by oxygen deficiency and sapropels did not form at all. At 6.7 Ma, the increasing restriction and sensitivity of the Mediterranean resulted in an extremization of the surface water conditions. The latter

are well documented, up to the MSC onset, by planktic foraminifera (PF) assemblages, that are characterised by the dominance (up to 100%) of cold-eutrophic species during insolation minima and warm-oligotrophic species during insolation maxima (Blanc-Valleron et al., 2002; Sierro et al., 2003). Calcareous nannofossils (CN) show similar responses, but their assemblages are usually dominated by small and opportunistic reticulofenestrads (Flores et al., 2005; Kouwenhoven et al., 2006; Mancini et al., 2020). Several other taxa indicate the establishment of eutrophic sea surface conditions, which were variably linked to more humid (*Helicosphaera carteri*) or arid (*Umbilicosphaera jafari*) climate (Flores et al., 2003; Mancini et al., 2020). *Sphenolithus abies*, instead, may be present (rarely abundant) during phases of water column stratification during warm climatic phases (insolation maxima, e.g. Tokhni, Gennari et al., 2018). However, *S. abies* is only peaking at the MSC onset (e.g. Fananello borehole, Manzi et al., 2007; Lozar and Negri, 2019; Figs. 1, 2), or it is regularly associated with each pre-evaporitic sapropel (e.g. Perales and Tokhni sections, Gennari et al., 2018; Mancini et al., 2020; Figs. 1, 2). The “amplification phase” (sensu Corbí et al., 2020) of the restriction starts at 6.75 Ma, when several micropaleontological changes occurred (Fig. 2). *Coccolithus pelagicus*, among CN, and the deep dweller *Globorotalia*, among PF, were strongly reduced just after 6.5 Ma (Blanc-Valleron et al., 2002; Sierro et al., 2003; Kouwenhoven et al., 2006). The latter event was tentatively linked to decreasing oceanic influence (Sierro et al., 2003). Following that, a major turnover of the cold-eutrophic PF stock occurred, and *G. bulloides* was replaced with turborotalids, a group associated to cooler sea surface temperature and variable marine salinities in modern ocean (Kroon et al., 1988; Schiebel and Hemleben, 2017). With the “consolidation phase” (sensu Corbí et al., 2020), from 6.35 Ma, the seafloor of many basins started to oscillate from strongly eutrophic to permanently anoxic (Fig. 2), as attested by the abundance increase of benthic foraminifera (BF) adapted to high nutrient/low oxygen levels during phase of insolation minima (Sierro et al., 2003; Kouwenhoven et al., 2006; Gennari et al., 2018), except in the Falconara section, where BF are almost absent (Blanc-Valleron et al., 2002). During this phase, another turnover was expressed by the increasing abundance of *Orbulina universa*, a morpho-species living today in different environments (Schiebel and Hemleben, 2017), at the expense of the *Globigerinoides* gr., a group preferring warm and oligotrophic conditions (Schiebel and Hemleben, 2017). This turnover occurred at ca 6.2 Ma, and roughly coincides with a phase of sediment instability (slumping, deposition of conglomerates, increase in sedimentation rate; Fig. 2) and a reduction from higher than normal to normal sea surface water salinity documented in the Ionian basin (Kontakiotis et al., 2022). Sedimentological and micropaleontological studies attest a series of changes predating the MSC onset. Laminated carbonates in the Eastern and Central Mediterranean (Zachariasse and Lourens, 2022) and the anomalously organic rich UA34 cycle in the Sorbas basin (Mancini et al., 2020) mark the onset of a sequence of almost monospecific CN peaks that were grouped and labelled as the CN MSC onset bioevents (event 20 in Fig. 2; Lozar and Negri, 2019; Mancini et al., 2020), interpreted as the final phase of eutrophication and restriction of the Mediterranean before the precipitation of gypsum. The paleoenvironmental change at the MSC onset (“climax phase” sensu Corbí et al., 2020) is also commonly marked by the disappearance of calcareous microfossils (Manzi et al., 2007; Gennari et al., 2013; Manzi et al., 2013, 2018; Gennari et al., 2018; Mancini et al., 2022) or a reduction of their size (Mancini et al., 2021; Corbí and Soria, 2016; Lirer et al., 2019) and the occurrence of euryhaline benthic foraminifera (Corbí and Soria, 2016). However, since foraminifera and CN may disappear slightly before the MSC onset (Govone section, Gennari et al., 2020), it has been recently suggested that a taphonomic bias could be in part responsible for their absence (Mancini et al., 2022).

2.3. Flora, vegetation, and climate on the Mediterranean borders

During the Late Miocene, the Mediterranean terrestrial landscapes

were still dominated by subtropical to temperate vegetal formations according to plant macroremains and palynological data (e.g. Bertini and Martinetto, 2011); their main components (e.g. *Taxodium*, *Glyptostrobus*, *Engelhardia*, *Carya*, *Quercus*) have today a disjoint geographic distribution (e.g. Europe, Asia and/or America). Palynological analyses along with pollen climate quantifications (Climatic Amplitude Method/CAM; Fauquette et al., 1998a, 1998b) contributed to the definition of climate parameter values (T and P) and different biomes (Fauquette et al., 1999; Fauquette et al., 2006; Bertini and Martinetto, 2008, 2011), whose distribution attested the occurrence of distinct climatic gradients marked by usually higher humidity in the north and increasing aridity in the southern Mediterranean area. The floristic and vegetational documentation of the pre-evaporitic MSC interval pertains to quite sparse Mediterranean pollen sites (e.g. Suc and Bessaïs, 1990; Suc et al., 1995; Fauquette et al., 2006 and references therein; Manzi et al., 2007; Gennari et al., 2013; Jiménez-Moreno et al., 2013; Bertini and Menichetti, 2015; Casas-Gallego et al., 2015; Suc et al., 2018) (Fig. 1) as summarized below. In the south-western MR, pollen studies were carried out in North Africa (Douiet 1 and MSD 1), eastern Spain (Venta del Moro, near Valencia) and Italy (Capodarso); some sites under the influence of the Atlantic regime were also studied, e.g. Bou Regreg (North Africa), Carmona and Montemayor-1 core, in lower Guadalquivir basin (Southern Spain). In this southern-western area, pollen assemblages pointed out an overall warm-xeric climate with contrasting seasons, as attested by the dominance of xerophytes (mainly herbs) plus some tropical pollen taxa during the time interval preceding the onset of the MSC. Herbs are, in fact, usually abundant, especially Poaceae and Asteraceae plus some sub-desertic taxa (e.g. *Lygeum* and *Neurada*). Among trees, *Pinus* is usually abundant; taxa typical of subtropical to warm temperate climate (e.g. Taxodioideae, *Myrica*, Cyrillaceae-Clethraceae, *Engelhardia*, *Cephalanthus*, *Pterocarya*, *Nyssa*, *Carya*) are also present, but generally subordinate to the non-arboreal ones. Climate quantifications on selected sites from this region estimated Most Likely Values (MLV) for mean annual temperatures (TA) around 20–22 °C and mean annual precipitation (PA) between 450 and 500 mm (Fauquette et al., 2006). At Can Villella, in the La Cerdanya basin (Spain), at NE of the previous area (Fig. 1), a riparian forest environment (Taxodioideae, *Alnus*, *Myrica*, Cyrillaceae-Clethraceae, *Engelhardia*, *Cephalanthus*, *Pterocarya*, *Populus*, *Nyssa*, *Salix*, etc.) with many herbs typical of local edaphic conditions (e.g. Cyperaceae, Poaceae and *Typha*) was associated to a prevalent warm and humid climate with MLV of TA and PA of 17 °C and 1150 mm, respectively. Pre-MSC pollen records were also collected from some well calibrated sections located on the Adriatic side of Northern Apennines (at Legnagnone, Fanantello and Trave). In the Trave section, the pollen record attests the dominance of subtropical to warm/temperate climates under an overall high humidity, between 7.61 and 6.33 Ma, despite some cooler episodes, marked by increases in *meso* to microthermic forest taxa (*Tsuga*, *Cedrus*, *Abies* and *Picea*); with herbs decisively subordinate (Bertini and Menichetti, 2015). Similar vegetal assemblages were also described at both Fanantello (Manzi et al., 2007) and Legnagnone (Gennari et al., 2013). The available climate quantification estimated, for the interval between 7.6 and 7.3 Ma, at Trave, a MLV of 17.5 °C; similar values (i.e. MLV around 17.8 °C) were obtained at Legnagnone at ca 6.12 Ma (Fauquette et al., 2015). In the Black Sea, pollen data from the DSDP Site 380 A attested a forested environment, dominated by subtropical to warm temperate taxa such as *Engelhardia*, *Myrica*, *Distylium* cf. *sinensis*, Taxodioideae, Sapotaceae, etc. Herbs, especially steppe taxa (mainly *Artemisia*) show a significant increase solely later, in the Pliocene. In this area the climate was warm and humid at the beginning of the Messinian with MLV of TA around 17.3 °C. PA was with a MLV around 1200–1300 mm (Fauquette et al., 2006).

Previous pollen data and their climate quantification allow the description of the floristic and vegetal landscape as well as the climate context associated to 3 biomes, i.e. broad-leaved evergreen-warm mixed forest, xerophytic woods-scrub, and warm grass-shrub biomes, which distribution permitted to trace different climatic gradients in the MR, at

least 1.6 Ma before the MSC onset (Suc et al., 1995; Bertini, 2006; Fauquette et al., 2006, 2007). Similar scenarios were formerly described for the earliest Pliocene (Fauquette et al., 1999, 2006). Specifically, the broad-leaved evergreen-warm mixed forest (TC: temperature of the coldest month, from 5° to 15.5 °C and E/PE with E: actual evapotranspiration, PE: potential evapotranspiration above 65%; Prentice et al., 1992), seems to be present in the Northern Apennines (Trave and Legnagnone), La Cerdanya basin (Can Villella), and Black Sea (DSDP Site 380 A). In all previous sites Taxodioideae forest is dominant. The other two biomes have an exclusive occurrence in the southern Mediterranean sites. The xerophytic woods-scrub biome is marked by TC above 5 °C and E/PE between 28 and 65%, and it is characterised by the dominance of tall xerophytic plants. The warm grass-shrub biome is typical of an open xeric environment and characterised climates with the temperature of the warmest month (TW) higher than 22 °C and a very low value of E/PE (between 18 and 28%). As a note for comparison, it is interesting to observe that the climate quantification of pollen records, for the interval between about 7.6 Ma and 5.9 Ma, estimated mean annual temperatures higher than today in the MR (Fauquette et al., 2006, 2007; Jiménez-Moreno et al., 2010).

3. Material and methods

Studies on pollen, dinocysts and calcareous nannoplankton have been carried out in the Messinian pre-evaporitic portion of the Govone section (Piedmont basin). They implemented former chronostratigraphical and biostratigraphical results focused on foraminifer data and allowed a comparison between the temporal variations of Earth's orbital parameters by using a cyclostratigraphic approach (Gennari et al., 2020 and references therein). The present investigations, performed on the same samples and including both terrestrial (pollen) and marine (dinocysts, foraminifera and calcareous nannoplankton) proxies, allowed direct land-sea correlations, and further insights into the main paleoenvironmental and paleoclimatic changes.

3.1. Site and materials

The Govone sedimentary section (44°48'08"N 8°07'34"E; Fig. 1) outcrops along the Tanaro River on the southern margin of the Piedmont basin, in its more distal exposed portion (Dela Pierre et al., 2011). It includes outer shelf to slope lower Messinian pre-evaporitic deposits (Sant'Agata Fossili Marls, SAF) formed between ca 6.6 Ma and 5.97 Ma (Gennari et al., 2020; Fig. 2), as well as the entire MSC sedimentary succession. The latter consists of primary gypsum deposits alternated with sapropels (Primary Lower Gypsum unit, Fig. 3a), clastic gypsum, slumped mudstones, and chaotic deposits (Valle Versa chaotic complex, Fig. 3b) and continental to lacustrine terrigenous sediments (Cassano Spinola Conglomerates) (Dela Pierre et al., 2016; Gennari et al., 2020; Sabino et al., 2020). The studied interval includes 31 lithological cycles in the SAF (Gm01 to Gm31), composed of couplets of brownish laminated sapropels and light grey massive marls (Gennari et al., 2020). Cycles are from <1 m up to 2 m thick (Fig. 3c), with a stacking pattern expressed by an alternation or cluster of thinner (0–15 m interval) and thicker (15–20 m interval) cycles (Fig. 2). A slump scar occurs at ca 27 m from the base of the section, marked by a 60 kyr sedimentary hiatus (Gennari et al., 2020). The onset of the MSC is placed, in the Govone section, at the base of the marls of cycle Gm30 according to Gennari et al. (2020) and Sabino et al. (2020) (Fig. 3d).

A minimum of 300 g of sediment was collected for each sample. At least one sample for each lithology (sapropel/marl) has been taken to document all semi-couplets. The current number of palynological samples (68) is lower than the micropaleontological ones (110); this deliberate decision was made to balance preparation time and associated costs while still achieving a total number that ensures adequate resolution. Quantitative analyses on foraminifera were already carried out (Gennari et al., 2020). New quantitative data concern calcareous

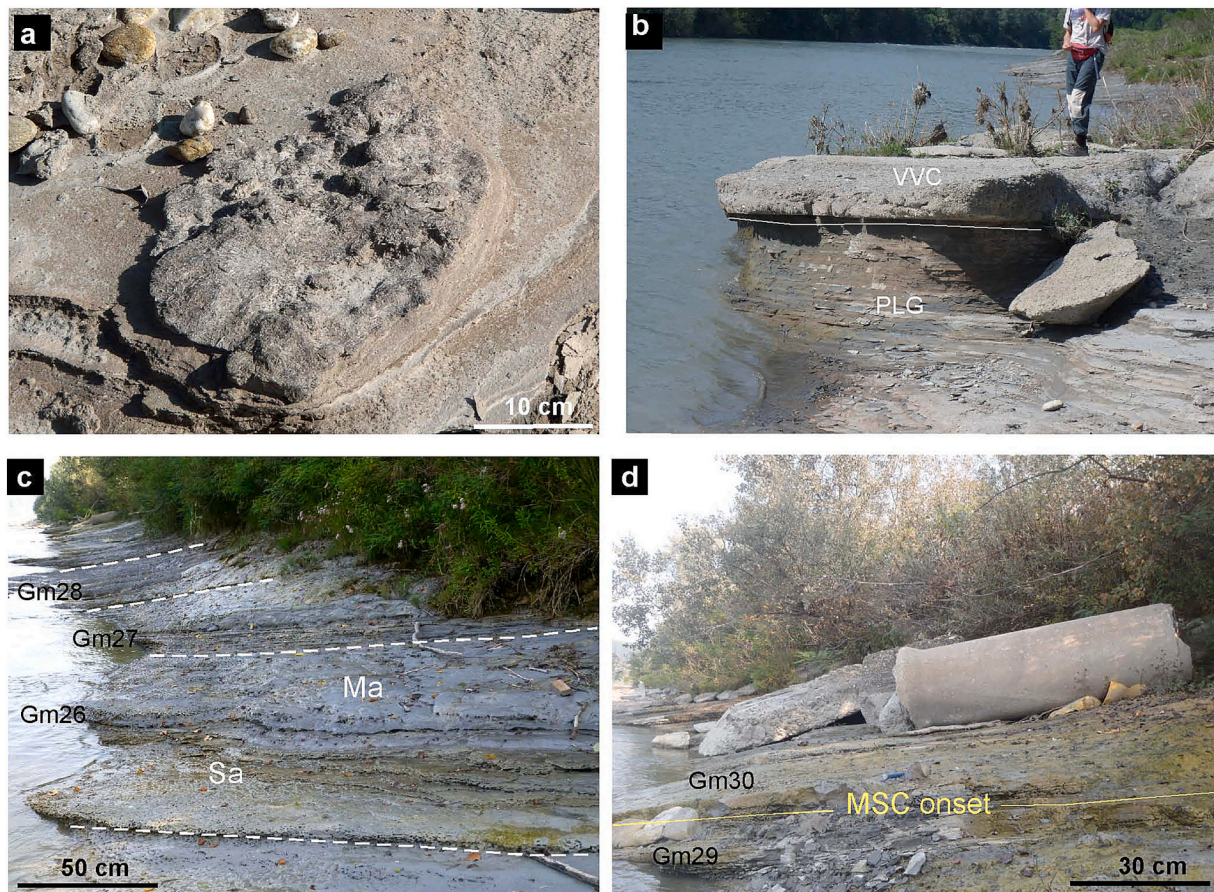


Fig. 3. Details of the sedimentary succession exposed at Govone (modified from Gennari et al., 2020). a) gypsum layer (Primary Lower Gypsum unit) consisting of flattened cones growing in a matrix of gypsiferous mudstones (see Natalicchio et al., 2021); b) the passage (white line) from the Primary Lower Gypsum unit (PLG) to the Valle Versa Chaotic complex (VVC); c) Lithological cycles in the Sant'Agata Fossili Marls (outlined by white dotted lines), consisting of laminated sapropel (Sa) / marls (Ma) couplets; d) the onset of the Messinian salinity crisis (MSC) at the base of marls of cycle Gm30.

nannoplankton and among palynomorphs, pollen and dinocysts (organic-walled resting cysts of planktonic dinoflagellates).

3.2. Calcareous nannoplankton

For calcareous nannoplankton analyses 110 sub-samples were prepared and investigated. Standard techniques for smear slide preparation allowed to retain the original composition of the sediments (Bown and Young, 1998). Observations at 1250 magnification were performed under cross-polarized light microscope, counting at least 500 specimens per slide, in order to assess the relative abundance of each taxon vs the total abundance.

3.3. Palynology

In total, 68 palynological sub-samples from SAF were analysed for their pollen and dinocysts content. From each sub-sample, 15 to 4.4 g were used for palynological analyses. The chemical-physical processing included treatment with HCl (10%) and HF (40%), $(\text{NaPO}_3)_6$, ZnCl_2 separation (solution density ca 2.0), sieving through a 10 μm mesh, and slides preparation using glycerol. Tablets containing an aliquot number of exotic spores (*Lycopodium*) were added to each sample, at the beginning of the preparation, to estimate the palynomorphs concentration. Residues were mounted in mobile slides, which were examined by transmitted-light optical microscope. Taxonomic identification conforms to reference collections and iconographic literature. For pollen identification, we referred to several publications (e.g. Martinetto et al., 2022; Niccolini et al., 2022), including pollen monographs (e.g. Pollen

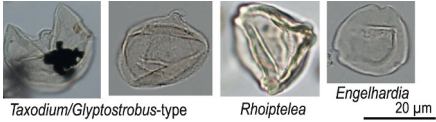
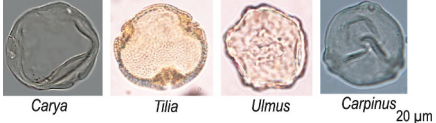
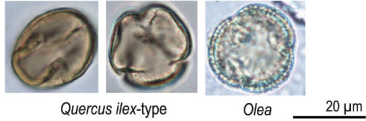
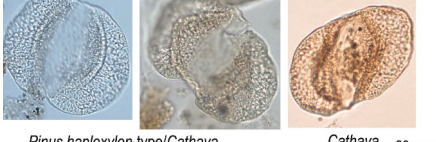
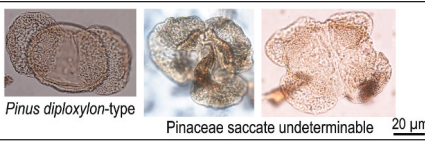
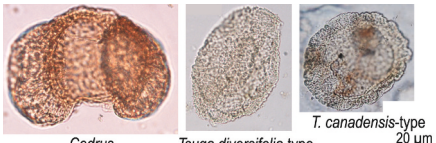
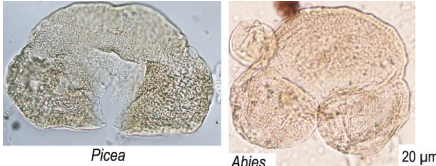

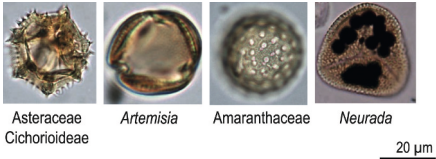
et Spores, Review of Palaeobotany and Palynology, Pollen et Spores d'Europe et d'Afrique du Nord by Reille, 1992). Additionally, we utilised the pollen reference collection at the Department of Earth Sciences at the University of Firenze. The results of pollen analysis are presented as: i. total pollen concentrations as well as ii. semi-detailed percentage diagram including most of the single pollen taxa and iii. summary percentage diagram, both plotted against depth; the summary percentage diagram includes nine different informal pollen groups based on the ecological and climate requirements of the corresponding modern taxa (Table 1). Data on dinocysts are presented as: i. total dinocysts concentration, ii. semi-detailed and iii. summary percentage diagrams. The *Spiniferites mirabilis* group includes *S. mirabilis* and *S. hyperacanthus*; the *Impagidinium* group includes *I. striatum*, *I. aculeatum*, *I. patulum*, and *I. velorum*. The most significant taxa or group of taxa have been also plotted. The occurrence of organic matter, Pteridophyta, microcharcoal and other Non-Pollen Palynomorphs - NPPs (Foraminiferal organic linings, *Pediastrum*, *Tasmanaceae*, *Pterospemella*) is specified on the left of the summary pollen diagram.

4. Results

4.1. Calcareous nannoplankton

The calcareous nannoplankton assemblage (Fig. 4) is dominated by the genus *Reticulofenestra*, either as *R. minuta* (a small reticulofenestrid <3 μm in size, which shows up to 80% of the assemblage in the sapropel of cycles Gm04–05, Gm09–10, Gm15, Gm21, and Gm27), or *R. haqii* (a larger reticulofenestrid in the range of >3 and < 5 μm , reaching

Table 1
Pollen groupings.

GROUPS	FLORAL ELEMENTS	MODERN CLIMATIC AND ECOLOGICAL SIGNIFICANCE	SELECTED POLLEN GRAINS
Subtropical humid forest taxa	<i>Arecaceae</i> , <i>Clethraceae</i> , <i>Cyrillaceae</i> , <i>Engelhardia</i> , <i>Myrica</i> , <i>Nyssa</i> , <i>Rhoiptelea</i> , <i>Sapotaceae</i> , <i>Sciadopitys</i> , <i>Sequoia</i> , <i>Taxodium</i> / <i>Glyptostrobus</i> -type (main component)...	Subtropical humid forest taxa: mega-mesothermic trees living under a climatic regime with a small range of temperature and abundant and well distributed rainfall throughout the year, typical of humid subtropical climate. Swamp taxa mainly belong to <i>Taxodiaceae</i> .	 <i>Taxodium</i> / <i>Glyptostrobus</i> -type <i>Rhoiptelea</i> <i>Engelhardia</i> 20 μm
Temperate broad-leaved deciduous forest taxa	<i>Acer</i> , <i>Buxus</i> , <i>Carpinus</i> , <i>Carya</i> , <i>Castanea</i> , <i>Celtis</i> , <i>Fraxinus</i> , <i>Juglans</i> , <i>Liquidambar</i> , <i>Parrotia</i> , <i>Pterocarya</i> , <i>Tilia</i> , <i>Quercus</i> , <i>Ulmus</i> , <i>Zelkova</i> ...	Mesothermic trees living under a climatic regime with adequate precipitation in all months; they withstand a strong annual temperature cycle with a cold winter season and a warm summer season (Warmer continental and humid subtropical climates).	 <i>Carya</i> <i>Tilia</i> <i>Ulmus</i> <i>Carpinus</i> 20 μm
Sclerophyll forest taxa	<i>Olea</i> , <i>Phillyrea</i> , <i>Pistacia</i> , <i>Quercus ilex</i> -type,...	Xerophilous hard-leaved trees and shrubs, which are typical of regions with a wet winter and dry summer (Mediterranean climate).	 <i>Quercus ilex</i> -type <i>Olea</i> 20 μm
<i>Cathaya</i> + <i>Pinus haploxyton</i> -type	Single components	<i>Cathaya</i> is a mesothermic gymnosperm now restricted in the humid, warm-temperate to subtropical areas of China.	 <i>Pinus haploxyton</i> -type/ <i>Cathaya</i> <i>Cathaya</i> 20 μm
<i>Pinus diploxyton</i> -type + <i>Pinaceae</i> saccate undeterminable	Single components	<i>Pinus diploxyton</i> -type includes numerous species with different ecologic and climatic requirements, due to the difficulty of its pollen grains to be determined below the genus level.	 <i>Pinus diploxyton</i> -type <i>Pinaceae</i> saccate undeterminable 20 μm
<i>Tsuga</i> + <i>Cedrus</i>	Single components	Mesothermic and meso-microthermic gymnosperms (mid-altitude elements) which demand humidity.	 <i>Cedrus</i> <i>Tsuga diversifolia</i> -type <i>T. canadensis</i> -type 20 μm
<i>Abies</i> , <i>Picea</i> , <i>Fagus</i> , and <i>Betula</i>	Single components	Microthermic needleleaf, coniferous trees (<i>Abies</i> and <i>Picea</i>), they are the dominant plants of the boreal forest, corresponding to subarctic and cold continental climates characterized by cold summer and long winter with year-long humid conditions. Broad-leaved deciduous trees and shrubs (<i>Fagus</i> and <i>Betula</i>) can be members of the early successional stages. This forest extends into lower latitude wherever mountains chains are present.	 <i>Picea</i> <i>Abies</i> 20 μm
Other arboreal taxa	<i>Alnus</i> , <i>Cupressoidae</i> , <i>Platanus</i> , <i>Populus</i> , <i>Salix</i> , plus indeterminate and undeterminable pollen grains	Taxa not climatically significant, often indicative of local edaphic conditions.	 <i>Alnus</i> <i>Cupressoidae</i> 20 μm
Non arboreal taxa	<i>Amaranthaceae</i> , <i>Asteraceae</i> (<i>Artemisia</i> included), <i>Apiaceae</i> , <i>Brassicaceae</i> , <i>Caryophyllaceae</i> , <i>Ericaceae</i> , <i>Euphorbiaceae</i> , <i>Fabaceae</i> , <i>Neurada</i> , <i>Poaceae</i> ...	The group comprises predominantly cosmopolitan taxa.	 <i>Asteraceae</i> <i>Cichorioideae</i> <i>Artemisia</i> <i>Amaranthaceae</i> <i>Neurada</i> 20 μm

percentages up to 70% in the sapropel of cycles Gm07, Gm11, Gm16–17, Gm23–25). Also abundant in discrete cycles is *U. jafari*, showing peaks up to 38% in the upper marls-lower sapropels of cycles Gm01–02, up to 50% in the marls of cycles Gm12–14, up to 59% in the marls of Gm23 and Gm25, where it reaches up to 41%. *H. carteri* reaches higher abundances, up to 30%, in the marls of cycles Gm05, Gm10, Gm18, Gm20, Gm22, Gm24, and Gm27. *Pontosphaera* spp. show a discontinuous record, with highest abundances up to 25% and with major peaks in the marls of cycles Gm08, Gm18, Gm20, Gm21, and Gm24.

Coccolithus pelagicus is common in the marls, in the lower half of the section (up to 25% in cycle Gm02 and Gm05) and shows a decreasing trend from the bottom of the section up to cycle Gm14; above this bed, it never reaches abundance higher than 5–7%. *Discoaster variabilis* is also more abundant in the lower part of the section, reaching 20% in abundance in cycle Gm03; it is a minor component of the assemblages in the upper cycles, never exceeding 2% in abundance. *Calcidiscus leptoporus* abundance is high (up to 75%) in the marls of cycle Gm23. *Reticulofenestra perplexa* shows a continuous but low abundance throughout

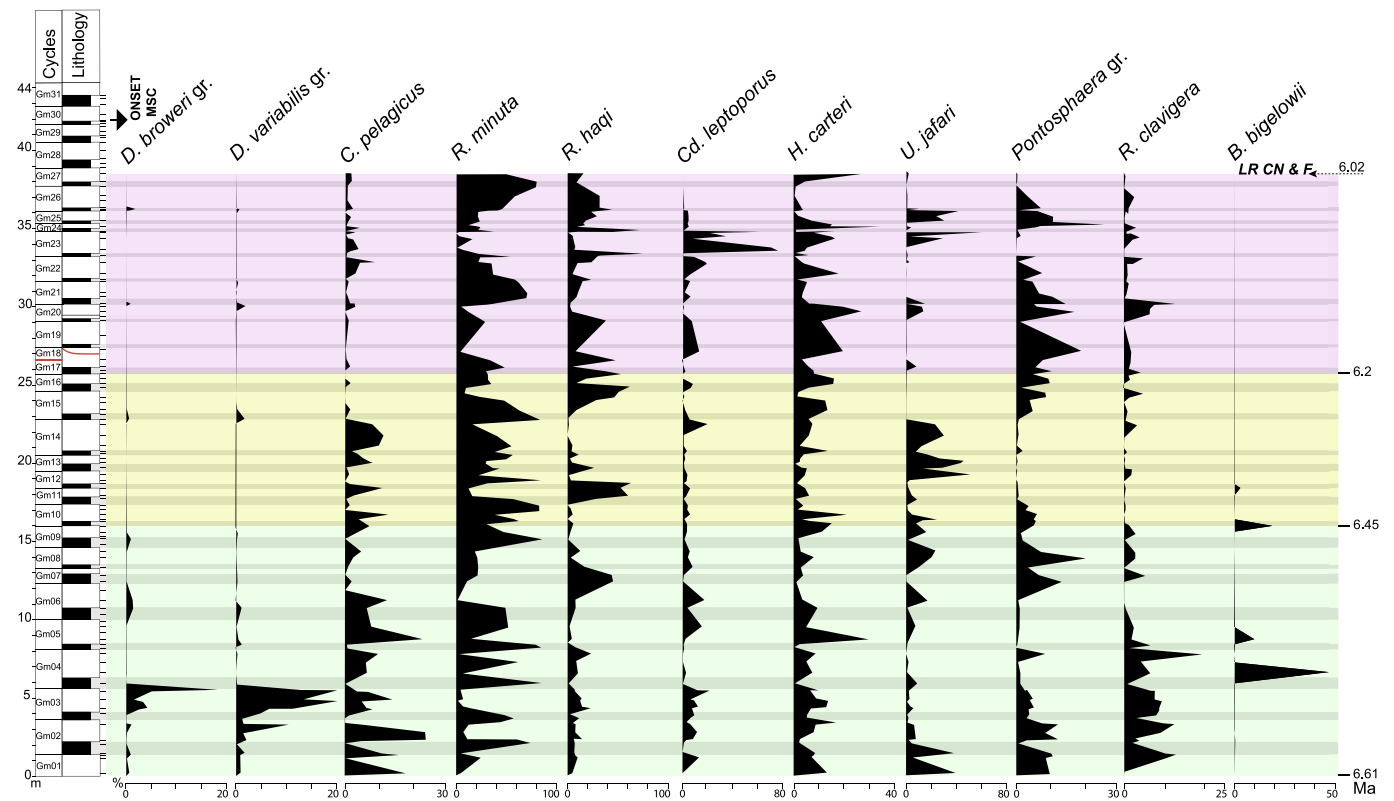


Fig. 4. Relative abundances of selected Calcareous Nannoplankton species. LR CN & F: last recovery of calcareous nannofossils and foraminifers. MSC: Messinian Salinity Crisis.

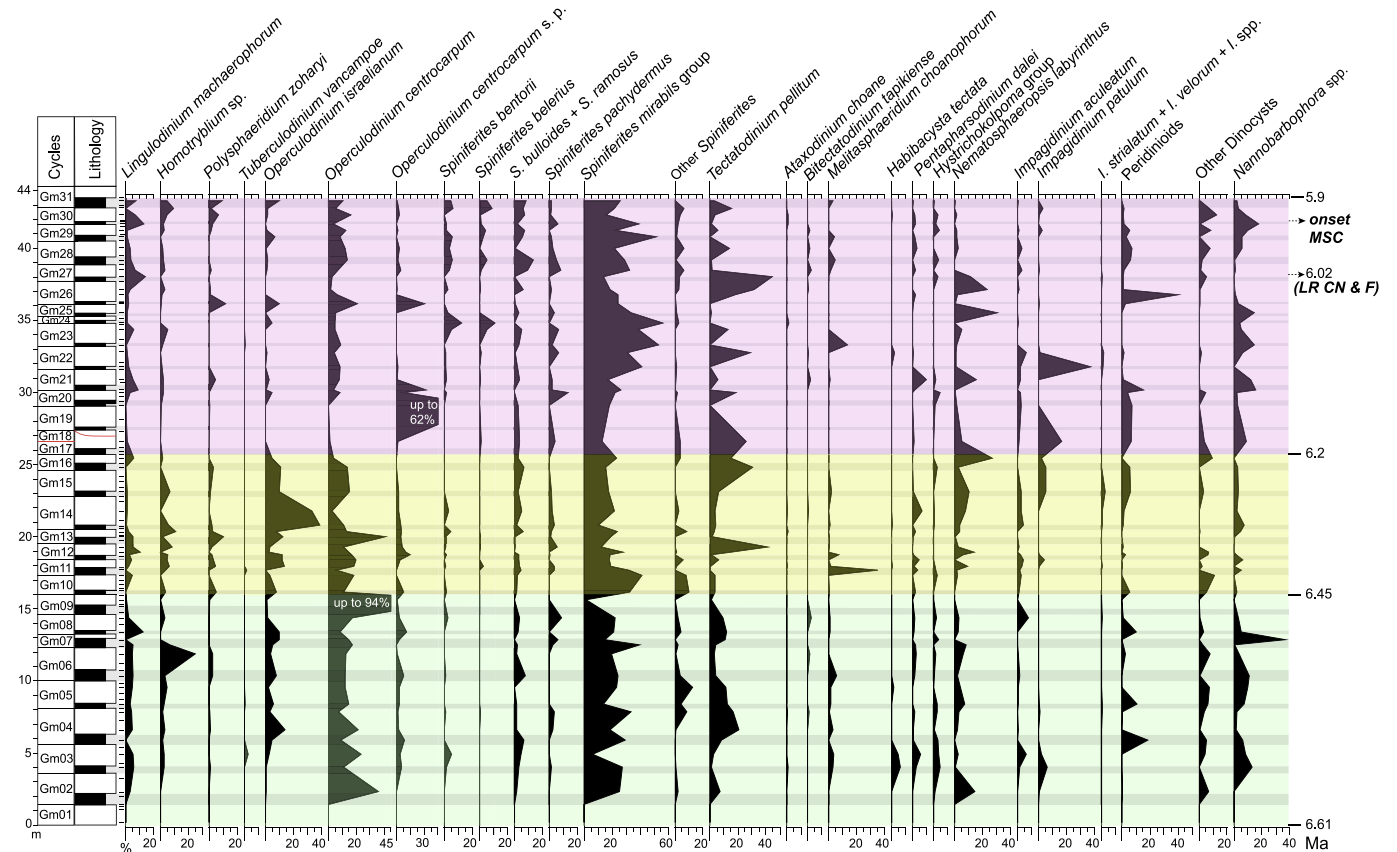


Fig. 5. Semi-detailed dinocysts diagram of the Govone section. The acritarch *Nannobarbophora* has been included in the basal sum. *O. centrocarpum* s. p. = *Operculodinium centrocarpum* morphotype short processes. LR CN & F: last recovery of calcareous nannofossils and foraminifers. MSC: Messinian Salinity Crisis.

the section (2 to 7%). Finally, *Sphenolithus abies* is a minor component of the assemblage (2–3%) and reaches higher abundances only in cycle Gm22 (10%). Three notable peak abundances of *Braarudosphaera bigelowii* occur at the base of the marls in cycle Gm04 (47.02%), in cycle Gm05 (10.22%), and in the sapropel of cycle Gm10 (19.4%). CN are last recorded in the basal portion of the marl of cycle Gm27.

4.2. Palynomorphs

4.2.1. Dinocysts

The record covers all the studied interval, except for 17 barren samples (cycle Gm01; marls in cycles Gm02, Gm06, Gm10, Gm14, Gm15, Gm17, Gm19, Gm24 and sapropels in cycles Gm09, Gm13, Gm27, Gm29) (Figs. 5–6). The counting of dinocysts ranges from 120 to 1640. Well-preserved dinocyst assemblages allow the identification of 50 taxa. However, their concentration is often low, ranging between 150 and 18,127 cysts/g. Assemblages exhibit a greater presence of autotrophic dinoflagellate cysts than heterotrophic ones. The most abundant and continuous taxa, besides marine acritarch genus *Nannobarbophora* spp., are *Operculodinium centrocarpum*, *Operculodinium israelianum*, *Homotryblium* sp., *Lingulodinium machaerophorum*, *Nematosphaeropsis labyrinthus*, *Spiniferites mirabilis*, *Spiniferites hyperacanthus*, *Tectatodinium pellitum*. Discontinuous taxa but with some significant peaks are *Selenopemphix brevispinosa*, *Operculodinium centrocarpum* morphotypes with short processes, *Melitasphaeridium choanophorum*, *Impagidinium patulum*, *Polysphaeridium zoharyi*, *Spiniferites pachydermus*, *Spiniferites belerius*, *Spiniferites bulloides*. Follow intermittently and/or with a low percentage *Impagidinium aculeatum*, *Pentaparsodinium dalei*, *Spiniferites* sp., *Spiniferites bentorii*, and *Spiniferites ramosus*. Sporadic cysts of *Selenopemphix quanta*, *Selenopemphix armageddonensis*, *Tuberculodinium vancampoeae*, *Impagidinium striatum*, *Impagidinium* sp., *Hystrichokolpoma cinctum*, *Hystrichokolpoma rigaudiae*, *Invertocysta* sp., *Spiniferites elongatus*, *Spiniferites delicatus*, *Spiniferites membranaceus*, *Achomospaera andalusiense*, *Achomospaera* sp., *Habibacysta tectata*, *Bitectatodinium tepikiense*, *Ataxodinium choane*, *Reticulospaera* sp., *Hystrichosphaeropsis obscura*,

Quadrina cf. *condita*, *Lejeunecysta* sp., *Echinodinium* sp., *Pyxidinospis* sp., *Polykrikos* sp., round brown, *Xandarodinium xanthum*, *Cerebrocysta* sp. are also observed.

When considering the distribution and abundance of the different dinocysts, it is possible to define some prevalent and distinct pattern within the sapropel-marl couplets. The dinocysts assemblages from marls are characterised, with respect to those from sapropels, by higher percentages of: i. *O. centrocarpum* (except in cycles Gm05, Gm12, Gm14–16, Gm22–24, Gm26, Gm28), with a maximum peak at 94% in cycle Gm09; ii. *N. labyrinthus*; iii. *P. dalei* (except in cycles Gm11, Gm12, Gm29); iv. *Homotryblium* sp. (except in cycles Gm10; Gm14–15; Gm22 in which is absent in the marls and in cycle Gm28 where it is much more abundant in the sapropel); v. *L. machaerophorum* (except in cycles Gm08, Gm21–22, Gm28–29); vi. *T. pellitum* (except in cycles Gm05–06, Gm08, Gm11, Gm14, Gm16). *H. tectata* (except in Gm03 and Gm14) and *B. tepikiense* are also present despite as punctuated occurrence.

Dinocyst assemblages from sapropels are characterised, with respect to those from marls, by higher percentage of: i. *S. mirabilis* group (except in Gm04–05, Gm08, Gm10, Gm12, Gm14, Gm16); ii. *O. centrocarpum* short processes (except in Gm28–30); iii. *M. choanophorum* with a maximum in the Gm11 (35%); iv. *O. israelianum* (except in cycles Gm03–04 and Gm11); v. *Impagidinium* group (except in cycles Gm03, Gm07–08, Gm26–31 in which are present with lower percentage in the marls and absent in the sapropels); vi. *Nannobarbophora* spp. (except in Gm05, Gm13, Gm17, Gm22, Gm27–29). vii. Peridinoids except in cycles Gm26–31.

4.2.2. Pollen

The rich and well-preserved palynoflora consist of 116 pollen taxa (Figs. 7, 8; Table 1). Pollen grains exhibit good overall preservation, though there are instances of corrosion observed in Pinaceae. The presence of charcoal and pyrite in some levels (anoxic) is noteworthy; in particular, pyrite, sometimes masking the morphological characteristics of some granules, prevented their identification. Except for 3 barren samples, 65 samples permitted the counting of pollen grains (range:

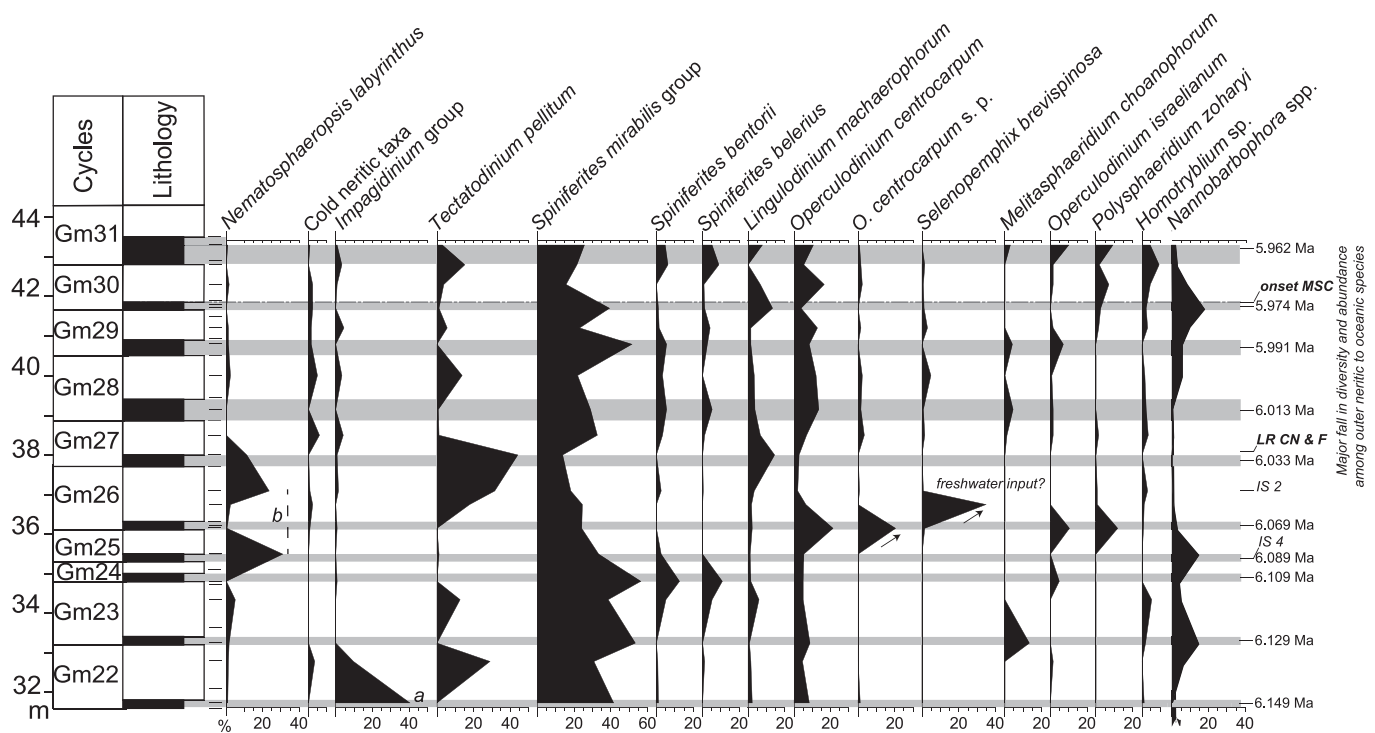


Fig. 6. Selected dinocysts curves for the interval between cycles Gm22 and Gm31 in the Govone section. *O. centrocarpum* s. p. = *Operculodinium centrocarpum* morphotype short processes. a: last significant influx of the full oceanic warm-water *Impagidinium* group; b: interval including the last two significant influxes of *N. labyrinthus* (neritic-oceanic cold-water). IS: Isotopic stage; LR CN & F: last recovery of calcareous nannofossils and foraminifers; MSC: Messinian Salinity Crisis.

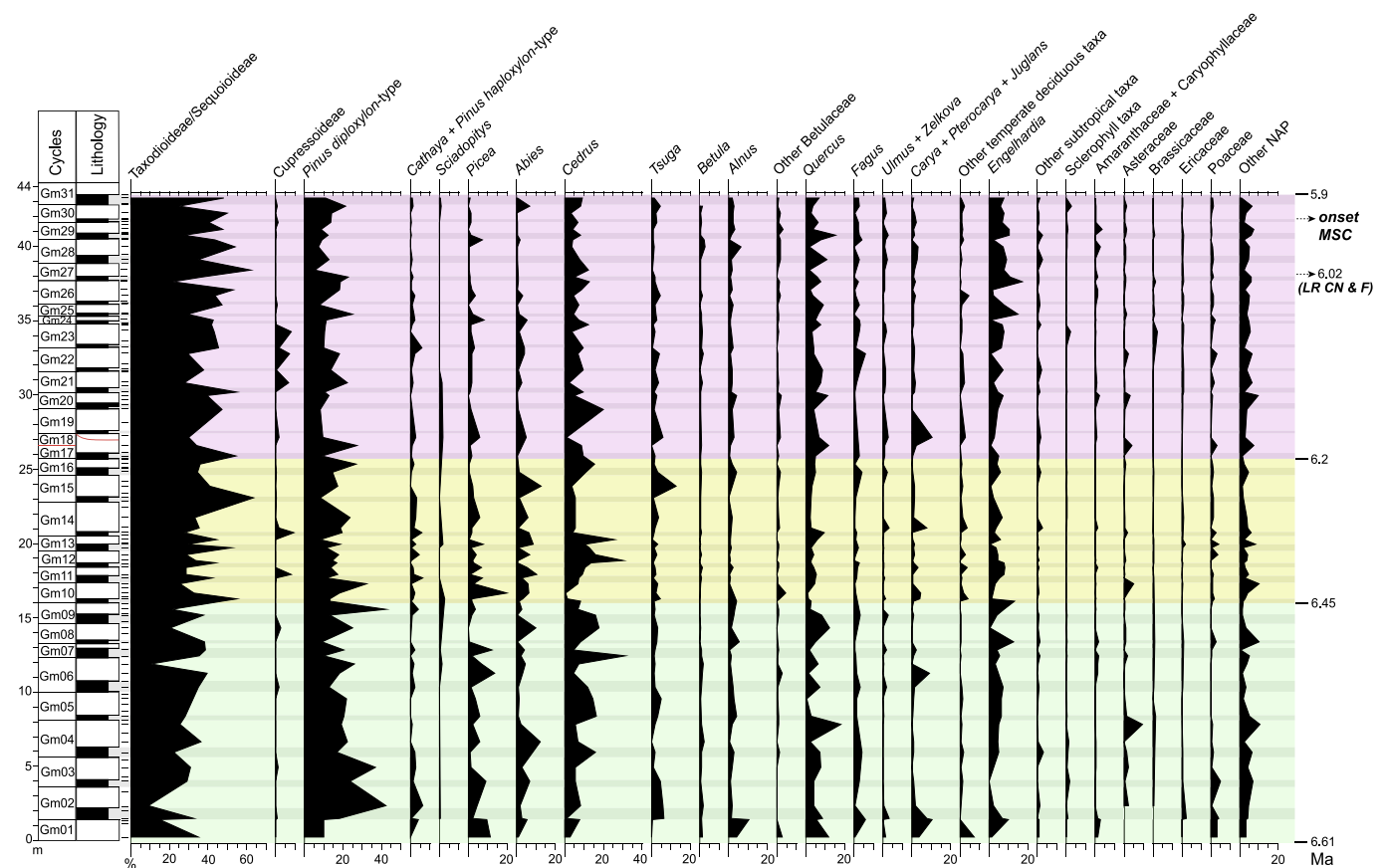


Fig. 7. Semi-detailed pollen diagram of the Govone section. LR CN & F: last recovery of calcareous nannofossils and foraminifers; MSC: Messinian Salinity Crisis.

94–1294). Total pollen concentration ranges from 146 to 484,397 grains/g. *Pinus* concentration ranges between 30 and 39,982 grains/g. Pollen assemblages exhibit a great number of taxa nowadays having an extra-Mediterranean distribution such as Taxodioidae. The latter which are the most abundant component of the subtropical humid forest are followed by taxa today restricted to some geographical sectors of the Mediterranean area (such as *Liquidambar* and *Zelkova*) or having a current distribution in (south) Europe and North Africa (such *Quercus*, *Carpinus*, and *Abies*). Among Angiospermae different taxa belonging to Fagaceae (*Quercus*, *Fagus*, *Castanea*), Betulaceae (*Betula*, *Alnus*, *Ostrya*, *Carpinus*), Juglandaceae (*Carya*, *Juglans*, *Pterocarya*, *Engelhardia*) and *Myrica* are well represented. Hamamelidaceae (*Distylium*, *Hamamelis*, *Parrotia*), *Liquidambar*, *Tilia*, cf. *Craigia*, *Nyssa*, Ulmaceae (*Zelkova* and *Ulmus*), *Celtis* and Oleaceae (*Phillyrea*, *Olea*, *Ligustrum*, *Fraxinus*) are in low value. More sporadic are *Acer*, Anacardiaceae, *Microtropis fallax*, *Cephalanthus*, Araliaceae (*Hedera* included), Rosaceae, *Pistacia*, *Salix*, *Symplocos*, *Arecaceae*, *Buxus*, *Ilex*, *Rhoiptelea*, *Lonicera*, Magnoliaceae, *Populus*, Vitaceae (included *Vitis* and *Parthenocissus*). Among the non-arboreal taxa, strongly subordinated to the arboreal ones, the most abundant belong to Asteraceae Asteroideae, Asteraceae Cichorioideae, Poaceae, Ericaceae and Amaranthaceae. They are followed by *Artemisia*, Brassicaceae and Cyperaceae. More sporadic are Rutaceae, Boraginaceae, Caryophyllaceae, Cistaceae (*Helianthemum*), Caprifoliaceae, Geraniaceae, *Galium*, Fabaceae, Ranunculaceae, *Rumex*, *Poterium*, Apiaceae, Urticaceae, Gentianaceae, Malvaceae, Cornaceae, Campanulaceae, Plumbaginaceae (*Limonium*), Liliaceae, Convolvulaceae, *Neurada*. Hydro- and hygrophytes are sporadic and in low values: *Spartanium*, *Typha latifolia* and *Myriophyllum*. Among the NPPs, algae, trilete and monolete Pteridophyta spores are present.

The pollen content shows a long-term trend, superimposed to different patterns characterising the sapropel/marl cycles. Pollen assemblages from marls are more often characterised with respect to

sapropels, by: i. higher percentages of *Pinus* in all cycles with exception of the Gm23, Gm27 p.p.-29 p.p. ones; ii. lower total concentration; iii. lower percentage values of pollen of Taxodioidae with exception of Gm03–06 and Gm27–30.

Pollen assemblages from sapropels are more often characterised by: i. higher concentrations values than marls except in cycle Gm14 and almost the same values in cycles Gm03–04; ii. higher percentages of Taxodioidae with respect to the overlying marls (same couplet), except in cycles Gm04–06, Gm14, Gm16, Gm24, Gm27–30; the same is observed with respect to the underlying marls (except in cycles Gm14, Gm16, Gm18, Gm24–25, Gm28–31); iii. commonly <15% (except in cycles Gm03, Gm06, Gm12, Gm29) of high montane taxa.

5. Discussion

5.1. Timing and progression towards the MSC onset: the response of the water column and sedimentary environments

5.1.1.1. Interval I – 6.61 Ma to 6.45 Ma (cycles Gm01–Gm09). At Govone a quite restricted marine environment is documented from 6.61 Ma (e.g. [Dela Pierre et al., 2011, 2016](#)). At that time the Mediterranean already experienced two major steps of sea floor deoxygenation at 7.16 Ma and 6.7 Ma ([Fig. 2](#); e.g. [Sierro et al., 2001](#); [Krijgsman et al., 2004](#); [Kouwenhoven et al., 2006](#); [Morigi et al., 2007](#); [Gennari et al., 2018](#)). A shelf setting is coherent with both the low abundance in the marls of open marine CN taxa such as *D. variabilis*, *R. clavigera* and *C. pelagicus*, and the presence of the BF *H. boueana*, *Melonis* spp. and *Cibicidoides* spp. ([Gennari et al., 2020](#)). BF also suggest moderate oxygenation at the sea floor during phases of insolation minima. Dinocysts assemblages exhibit the predominance of neritic species (e.g. *Spiniferites* spp. and *T. pellitum*)

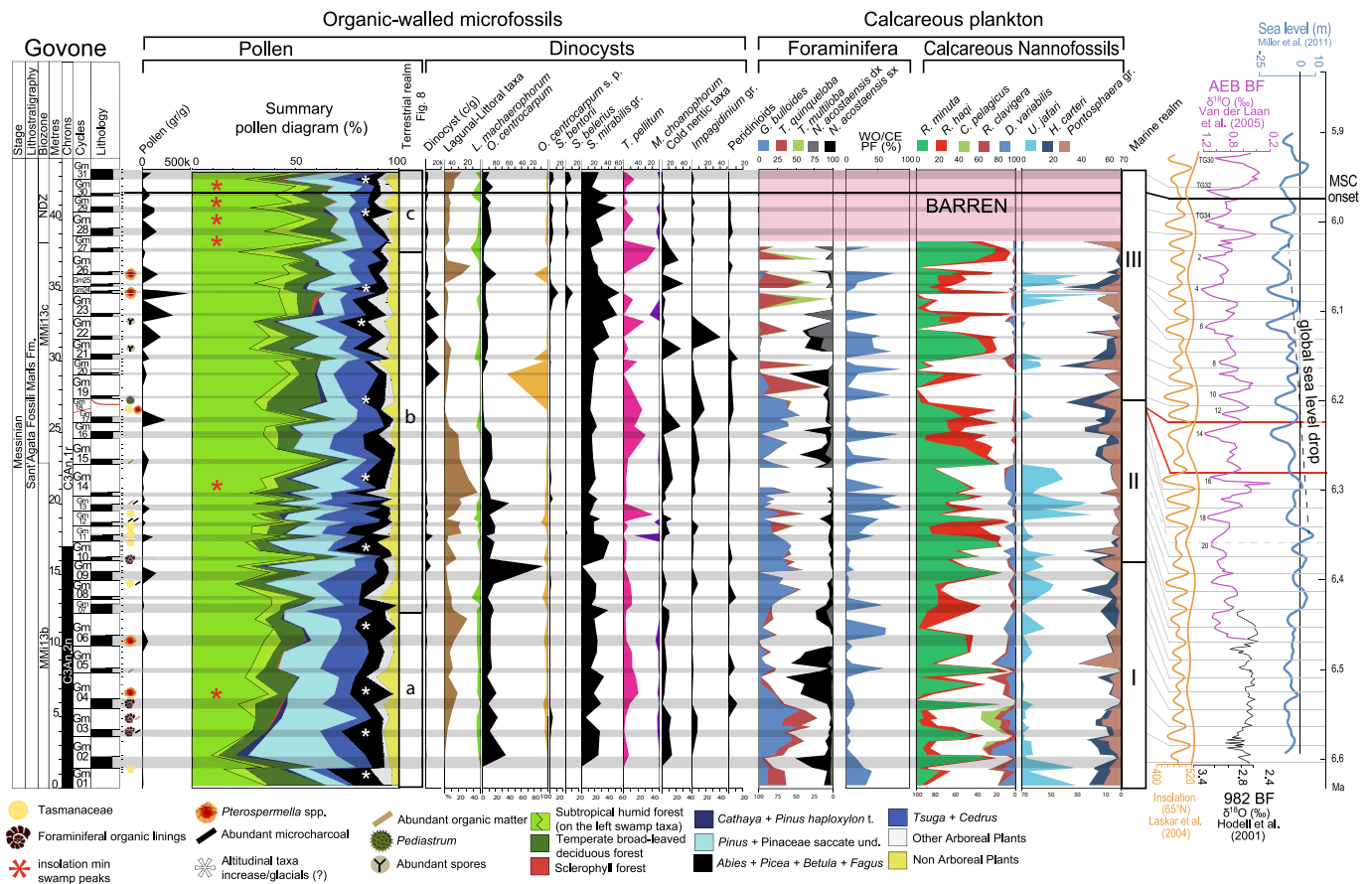


Fig. 8. Stratigraphic log of the Govone section and summary of the main terrestrial and marine stratigraphical data. On the right the curves of insolation at 65°N and eccentricity (Laskar et al., 2004); δ¹⁸O (AEB BF, van der Laan et al., 2005 and 982 BF, Hodell et al., 2001); Sea level in meter (Miller et al., 2011). LR CN & F: last recovery of calcareous nannofossils and foraminifers; MSC: Messinian Salinity Crisis.

on full oceanic ones (Figs. 5, 8). The latter mostly include the components of the *Impagidinium* group plus *N. labyrinthus*, a species having oceanic-neritic affinities. The inner neritic taxa progressively increase, from cycle Gm04; particularly the warm-water species, today typical of hypersaline lagoons, such as *O. israelianum*, *P. zoharyi*, *S. bentorii*, *Homotryblum* sp. (Fig. 5). In cycle Gm04 *B. bigelowii* also exhibits a prominent peak abundance; this taxon shows a strong affinity for coastal waters, at present (Duarte-Silva et al., 2004; Hagino et al., 2019) and in the past (Bartol et al., 2008). It is usually very rare or absent in offshore sediments (Okada and Honjo, 1973; Hagino et al., 2016) and it has been also related to low salinity environments (Bukry, 1974; Bartol et al., 2008) and nutrient enrichment (Peleo-Alampay et al., 1999). At the K/Pg boundary it shows ability to quickly diversify and adapt to changing environmental conditions, increased nutrient availability and strong competitor reduction (Jones et al., 2021). An additional precursor signal of the basin restriction is represented by the decrease of open ocean CN taxa (*D. variabilis*, *R. clavigeru* and *C. pelagicus*), in Gm05, at ca 6.5 Ma (Figs. 4, 8) and of the deep dwellers *G. miotumida*, which is rare and disappears at the end of the interval. *O. centrocarpum*, typical of transitional oceanic-neritic realms is quite abundant from cycle Gm02; today such species tolerates a wide range of salinity and sea surface temperature (e.g. Wall et al., 1977; Matsuoka, 1987; McMinn, 1991; Pospelova et al., 2005; Zonneveld et al., 2013; Zonneveld and Pospelova, 2015); its occurrence has been often linked to nutrient-enriched waters, and waters such as the North Atlantic Drift (Wall et al., 1977; Harland, 1983). At the top of the interval, at ca 6.45 Ma, close to the last regular occurrence (LrO) of *G. miotumida*, *O. centrocarpum* (94%, in Gm09) exhibits its major acme (Figs. 5, 8) close to the 400-kyr eccentricity minimum during low amplitude variations in summer insolation. Possibly it

corresponds to a freshwater input based on the observed increases of this taxon in regions where salinities are reduced as result of meltwater input during the summer season or due to river discharge (Zonneveld and Pospelova, 2015). Just at the base of the sapropel of cycle Gm10, a peak of *B. bigelowii* (19%) attests a strong instability and an environmental crisis for all competitors probably coinciding with the suggested salinity decrease. The repetitive freshwaters influxes contributed to the high nutrient levels, as also testified by the prevalent occurrence of eutrophic PF taxa (Fig. 8).

It is quite evident by marine bioindicators that the depositional basin was submitted to successive and rapid environmental changes especially affecting salinity levels already from 6.61 Ma.

In summary, for Interval I: since 6.61 Ma, Govone hosted a confined and dynamically unstable marine environment, characterised by fluctuating salinity values and enhanced seafloor oxygenation (at insolation minima), impacting the distribution of marine taxa. Assemblages underscore the dominance of neritic species over oceanic ones; dinocysts exhibit a progressive increase of inner warm-water neritic taxa. A potential freshwater input marks the top of the interval, around 6.45 Ma, coinciding with a decline in oceanic taxa.

5.1.1.2. Interval II – 6.45 Ma and 6.20 Ma (cycles Gm10-Gm16). After the restriction step, the general increase of thermophilic dinocysts attests a succession of warm phases, between 6.45 Ma and 6.34 Ma despite some cooler fluctuations (especially of *N. labyrinthus* and *P. dalei*) (Figs. 5, 8). The initial increase of the warm/oligotrophic *S. mirabilis* group (cycle Gm10) is followed by the expansions of several inner neritic taxa, such as *Melitasphaeridium choanophorum* at 6.43 Ma (cycle Gm11), the meso-eutrophic *T. pellitum* at 6.39 Ma (Gm12), and *O. israelianum*, at

ca 6.36 Ma (cycle Gm14) (Figs. 5, 8). The abundances of *O. israelianum* well above 10% attest SST exceeding 14.3 °C in winter and 24.2 °C in summer, with SSS ranging from 30 to 39.4 (winter-summer). The increase of bolivinids and buliminids, among BF, at ca 6.42 Ma (Gennari et al., 2020) as well as of *T. pellitum*, at 6.39 Ma, represents the bottom eutrophication step that also characterises the entire Mediterranean Sea, in response to increasing surface productivity during phases of insolation minima (e.g. Sierro et al., 2001; Filippelli et al., 2003; Krijgsman et al., 2004; Kouwenhoven et al., 2006; Morigi et al., 2007; Gennari et al., 2018). The change of the benthic assemblages coincides with the onset of regular oscillation of the ratio between warm and oligotrophic PF (WO) and colder and more eutrophic PF (CE) (maxima in sapropels and minima in the marls), interpreted as evidence of restriction and enhanced sensitivity to the climatic changes. The onset of the WO/CE ratio oscillation is delayed of approximately 300 kyr with respect to other Mediterranean basins (e.g. Sorbas, Sierro et al., 2003), where it starts at 6.7 Ma. The delay could be ascribed to the northern latitude of the Piedmont basin, which hindered the proliferation of the WO assemblage (Fig. 8) and promoted the CE group (*G. bulloides*, turborotalids and *N. acostaensis*). However, consistent with the warming suggested by dinocyst assemblages, WO PF peaks increase in frequency, too (Fig. 8).

Approaching the major global sea level drop (after 6.35 Ma) and the onset of heavier $\delta^{18}\text{O}$ positive excursions linked to the onset of the transient Northern Hemisphere (NH) glaciations (Hodell et al., 2001; van der Laan et al., 2005; Holbourn et al., 2018; Figs. 2, 8), the changes in CN assemblages attest an increase of surface runoff which, in turn, feeds the primary productivity in the water column and reinforces the eutrophication of the seafloor. *U. jafari*, usually associated to higher than normal marine salinity (Flores et al., 2003; Mancini et al., 2020), drops just before 6.3 Ma, in cycle Gm15, where also the abundance of the open ocean taxon *C. pelagicus* drops to its minimum. This change is parallel with the increase of *H. carteri* and the *Pontosphaera* gr. adapted to lower than marine salinity conditions (Dimiza et al., 2014; Bonomo et al., 2021). In concomitance, the right coiled neogloboquadrinids increase in abundance (Fig. 8), supporting the establishment of a deep chlorophyll maximum (Sierro et al., 2003; Schiebel and Hemleben, 2017) and stratified conditions promoted by the stronger influence of runoff.

In summary, for Interval II: after 6.45 Ma, rising thermophilic dinocysts and expanding inner neritic taxa attest warm phases with elevated SST and SSS. Simultaneously, increased bolivinids, buliminids, and *T. pellitum* mark the onset of bottom eutrophication. Close to the global sea level drop (after 6.35 Ma) changes in calcareous nannoplankton assemblages, reflects heightened surface runoff and intensified water column productivity, leading to seafloor eutrophication. Species adaptations suggest changing salinity conditions. Just before 6.3 Ma, alterations in neogloboquadrinids support the development of a deep chlorophyll maximum and stratified conditions influenced by increased runoff.

5.1.1.3. Interval III (6.20 Ma to 5.96 Ma (cycles Gm17-Gm31). The slump scar between cycles Gm17 and Gm18 (Fig. 8), is likely the local expression of a tectonic phase that also left traces in the Mediterranean area (Fig. 2). Among PF, *T. quinqueloba* and the Messinian ecomorphotype *T. multiloba* replace *G. bulloides* in the marls during insolation minima (Fig. 8). *T. quinqueloba* tolerates salinity and temperature excursions (Kroon et al., 1988) and thus can thrive in front of estuaries, where runoff brings both nutrient and low salinity waters to the sea (Ijiri et al., 2005). Moreover, it prefers cooler SST than *G. bulloides* (Schiebel and Hemleben, 2017). Freshwater inputs are particularly well attested among dinocysts by the increases at ca 6.18 Ma (cycle Gm20) and also later at ca 6.07 Ma (cycle Gm26) of *O. centrocarpum* short processes, a taxon usually associated to subnormal to hypohaline SSS (e.g. De Vernal et al., 1989; Nehring, 1994, 1997; Dale, 1996; Matthiessen and Brenner,

1996; Ellegaard, 2000; Brenner, 2001a, 2001b, 2005) (Figs. 5, 6, 8). The major peak of *O. centrocarpum* short processes (at ca 6.18 Ma; Fig. 8) is sandwiched between the last two significant influxes of the full oceanic warm-water *Impagidinium* group, respectively below the slump scar (before 6.2 Ma) and above it, at 6.14 Ma (in cycle Gm22; a in Fig. 6; Fig. 8). CN are largely dominated by taxa adapted to stressed marine conditions (*R. minuta*) and fluctuating marine salinities (*H. carteri* and *Pontosphaera* spp.); the presence of open ocean taxa is largely subordinated and episodes of raised marine salinity are represented by the peaks of *U. jafari*. These microfossil assemblages indicate that the paleo-environment was changing towards restricted condition characterised by SSS variations, while open marine conditions were re-established during relatively short intervals. It is worth noting that an enhanced water exchange between the Mediterranean and the Paratethys was suggested by Vasiliev et al. (2019) at 6.15 Ma; such an event can be tentatively related to the observed dinocyst event at ca 6.18 Ma and in general with the proliferation of taxa adapted to low salinity conditions, including the increase, among CN of *H. carteri*. The continuous salinity change in this interval is also supported by a short event characterised by the high abundance of *C. leptoporus*. This taxon, attesting mesotrophic to eutrophic conditions in cycle Gm23, exhibits broad ecological requirements, but a preference for nutrient-enriched waters and has been correlated with low salinity waters (Baumann et al., 2016). The oscillating restricted/open ocean mode continued up to the two influxes of the oceanic *N. labyrinthus*, centred at 6.08 and 6.05 Ma (cycles Gm25/Gm26; b in Fig. 6), within isotope stages 4 and 2 (van der Laan et al., 2005). They mark the arrival of the neritic-oceanic cold-water, in a more and more restricted environment as confirmed by *Homotryblum*, in the sapropel of cycle Gm26 (ca 6.075 Ma); the latter is followed by the successive increase of *P. zoharyi* and *O. israelianum* plus that of *O. centrocarpum* (including the short processes type). Such stressful environmental conditions possibly amplify global changes, marked by the increasing amplitude of the oceanic $\delta^{18}\text{O}$ (van der Laan et al., 2005). At ca 6.04 Ma, in the marls of cycle Gm26, a significant freshwater input could explain the major peak of *S. brevispinosa* (the major component in the Peridinioids curve of Figs. 5, 6, 8) an inner neritic species indicative of reduced salinity, in coincidence with the sudden decrease/or disappearance of some of high salinity taxa previously present (e.g. *O. israelianum*). These environmental conditions favour among the CN, *R. minuta*, a neritic, opportunistic species that tolerates variations of salinity. From cycle Gm27 a main peak in the inner neritic dinocyst *T. pellitum* is recorded as well as a quite good increase of *L. machaerophorum* (Figs. 5, 6, 8). In its correspondence the *Spiniferites* warm group, usually quite well represented, suffers a short-term decrease. At the same time among CN, *H. carteri* supports input of waters with variable salinity, close to the coast and near estuaries, with high nutrients. *Nannobarbophora*, an acritarch having warm water affinity (Head, 2003), shows a successive good increase which approximates the onset of the MSC placed at the base of the marls of cycle Gm30 (Gennari et al., 2020; Sabino et al., 2020). The uppermost interval, across the onset of the MSC, up to reach the sapropel semi-couplet of cycle Gm31, at 5.962 Ma, shows a quite good increase of dinocysts typical of coastal areas attesting extreme variations in salinity according to a trend defined by the succession within *Homotryblum*, *S. bentorii*, *O. israelianum* plus *P. zoharyi* (Figs. 5, 6, 8). In this contest, the last recovery (LR) of foraminifera and CN, calibrated at 6.02 Ma, in cycle Gm27 (Fig. 8), is surprising and uncommon in the stratigraphic record of the pre-evaporitic/MSC transition. In fact, CN usually mark the beginning of the crisis at 5.97 Ma with a succession of peaks of different taxa (Manzi et al., 2007; Lozar and Negri, 2019; Mancini et al., 2020). In marginal basins, PF can undergo an early decline with respect to BF (Gennari et al., 2013; Mancini et al., 2020), which disappear at the MSC onset. In the Eastern Mediterranean Gennari et al. (2018) documented a decrease in abundance of either PF or BF at 6.06 Ma, before their disappearance. The resilience of CN with respect to surface water salinity fluctuations is attested by their occurrence in brackish marginal seas (the Baltic and

Black seas, Bukry, 1974; Thomsen, 2016); in some context, like in the Western Mediterranean Bajo Segura basin, also foraminifera found suitable conditions to survive the MSC onset, although affected by the environmental stress, which led to dwarfism (Corbí et al., 2016). In view of these scenarios, probably influenced by the local response to the environmental deterioration, the lack of calcareous microfossil from 6.02 Ma in the Govone section is better explained with a taphonomic bias. This is confirmed by the occurrence of some dinocysts (including *Spiniferites*) across the LR of CN and F, indicating perduring fit conditions in the photic zone at least for CN, as occurring in the more marginal Pollenzo section (Dela Pierre et al., 2011), few kms to the west (Violanti et al., 2013). The good presence of *T. pellitum*, a taxon tolerating a wide range of bottom water oxygen, including anoxic conditions, suggests summer SST > 14.4 °C (and < 29.5 °C), with SSS ranging from 21.9 to 39.2 (winter-autumn) (Zonneveld and Pospelova, 2015) as well as high productivity. Paleoenvironmental reconstructions indicated the establishment of conditions that favoured stratification, as also supported by molecular proxies (Sabino et al., 2020) and dysoxic to anoxic bottom waters, which enhanced organic matter accumulation on the sea floor. These conditions favour the preservation of organic walled (pollen and dinocysts) versus calcareous microfossils, by producing excess CO₂ and acidification of the sediment pore waters via remineralization reactions (Sarmiento and Gruber, 2006).

In summary, for Interval III: from 6.2 Ma onward freshwater inputs are suggested by dinocysts at ca 6.18 Ma and 6.07 Ma. CN assemblages reflect rapid fluctuations between restricted and open marine conditions. Neritic to oceanic, and cold-water influxes between 6.08 Ma and 6.05 Ma precede heightened stress towards the MSC onset. At 6.02 Ma, CN and foraminifera disappear, while dinocysts persist, marking distinct phases characterised by frequent extreme salinity variations. Stratification and dysoxic to anoxic bottom waters promote organic matter accumulation, favouring the preservation of organic walled palynomorphs over calcareous microfossils.

5.1.2. The marine biological signature of the precession sedimentary cycles

As previously stated, fluctuations between warm/oligotrophic and cold/eutrophic calcareous plankton assemblages are well known in the pre-evaporitic successions of the Mediterranean and have been linked to climatic and oceanographic variations triggered by the precessional forcing (e.g. Hilgen and Krijgsman, 1999; Sierro et al., 2001; Blanc-Valleron et al., 2002; Kouwenhoven and van der Zwaan, 2006; Gennari et al., 2018; Lozar et al., 2018). At Govone, the cyclical expression of planktic microfossil assemblages is well defined. Gennari et al. (2020) documented 0–100% variation of the ratio of warm-oligotrophic (WO) to cold-eutrophic (CE) PF which are better expressed after 6.4 Ma (Fig. 8). Before that age, the variability of this ratio seems to be modulated by longer periods (plausibly eccentricity), as it shows an interval characterised by WO peaks during insolation maxima (Gm05–Gm07) sandwiched between intervals dominated by CE assemblages (Gm02–Gm04 and Gm08–Gm10). In general, calcareous plankton taxa associated to warm and oligotrophic conditions such as *O. universa*, among PF (WO group), and the opportunistic taxon *R. minuta* sometimes accompanied or substituted by *R. haqii* among CN, are dominant in the sapropels, where BF are particularly scarce or absent. For the first time in Messinian Mediterranean successions, we document, throughout several cycles, that also the dinocysts typical of warm-water assemblages are mostly dominant in sapropels (Figs. 5, 6, 8). Among them, the few oceanic taxa including the prevalent oligotrophic *Impagidinium* group, are rather discontinuous and subordinated to the others. On the other hands, warm neritic species are abundant (e.g. *S. mirabilis* group, *S. bentorii*, *O. israelianum*). *Nannobarbophora* spp. is often frequent and in sapropels it reaches some of its higher values (maximum value at ca 6.51 Ma, in cycle Gm07), including that in correspondence of the MSC onset (5.1.1.3.).

In contrast, in the marls, usually, PF assemblage representative of colder and more eutrophic environments (CE group) is associated with a

variable number of BF, which either show a predominance of oxyphilic species (up to cycle Gm19) or of taxa adapted to low oxygen levels/high food availability, which can thrive in sea-floor that receive a high export productivity (*Bolivina* and *Bulimina* groups; Murray, 2006; Kouwenhoven et al., 2003, 2006). The CN assemblages of the marly semi-couplets show distinct peaks of *C. pelagicus* (up to cycle Gm14), *H. carteri*, *U. jafari*, *C. leptoporus* and the *Pontosphaera* gr., suggesting high nutrient levels, temperate climate and a well-mixed water column. However, *U. jafari*, linked to raised salinity (Mancini et al., 2020), and the euryhaline taxa *H. carteri*/*Pontosphaera* gr. commonly alternates, possibly suggesting different nutrient sources (mixing or runoff, respectively). In marls, cold-water dinocysts are more frequent than in sapropels. They do not include full oceanic taxa, and only one species, *N. labyrinthus*, having neritic-oceanic affinities, is more often present and in higher values than in sapropels. Other cool water species (i.e. *P. dalei*, *B. tepikiense*, *H. tectata*) having a neritic distribution are also present. However, the common low abundance of cool-water species, including the spring-blooming species *P. dalei* cyst suggests prevalent warm spring temperatures and mild winter sea-surface temperatures, throughout the record. *O. centrocarpum* is also usually more frequent in marls than in sapropels; this taxon, as already discussed, exhibits high relative abundances in regions where salinities are reduced as result of meltwater input during the summer season or due to river discharge; possibly both conditions were satisfied in the Govone basin. *L. machaerophorum*, a temperate to tropical species, often found in stratified water, and interpreted as a proxy for fluvial discharges too, exhibits some major increases as well, in the marls. In this context, the significant peak of the warm (hypersaline) water *Homotryblum* sp. in the marls of cycle Gm06 (Fig. 5), at ca 6.52 Ma, possibly related with the phase of low-amplitude variance in obliquity node, during a minimum in eccentricity. From about 6 Ma (cycle Gm27), (oceanic) cold-water taxa suffer an overall major decrease, in coincidence with the last appearance above 10% of *N. labyrinthus*. The progressive shrinkage of the open marine conditions probably prevents a correct and comprehensive evaluation of cold-water phases, according to dinocysts evidence, because it caused a progressively reduction in the record of *N. labyrinthus*. Additional biases also related to the disappearance of stenohaline taxa due to the progressively affirmation of an environment strongly submitted either to drastic and frequent salinity changes or to an intensification of the water column stratification across the MSC onset.

5.2. The terrestrial realm

Pollen-based reconstructions provide the flora composition and vegetal structure of terrestrial ecosystems in the Piedmont region (Figs. 7, 8, 9). A rather exclusive arboreal cover distributed in lowland/coastal areas; here *Taxodium*, *Glyptostrobus* and other Taxodioidae thrived in freshwater swamps some of them probably part of a river system with bordering fan and talus deposits sourced from the surrounding Alpine chain. Other deciduous broadleaved trees taxa, such as *Salix*, *Alnus*, and *Fraxinus* were also present. *Engelhardia*, *Carya*, *Quercus*, and other subtropical to warm/warm temperate arboreal taxa expanded in well drained soils. In the close mid relieves of the Alpine chain, *Cedrus* and *Tsuga* thrived, whereas towards higher altitudinal belts *Betula*, *Fagus*, *Picea* and *Abies* extended. *Cathaya*, was also present at mid- to high altitudes. Today *Cathaya argyrophylla* CHUN ET KUANG (1962) is the only species in the genus and is endemic to China, where optimal habitats are those with an altitude between 758 m and 1500 m (Xiao et al., 2022).

The repeated increases of mid to high altitude arboreal taxa attest decreases of temperature but not of humidity, because of the absence of any concomitant rise of the open vegetation taxa. Some peaks of abundance of mid to high altitude arboreal taxa correlate with glacial phases in the isotopes curves as shown in Fig. 8. However, an overall decrease of the mid- to high altitude taxa is recorded from the bottom to the top of

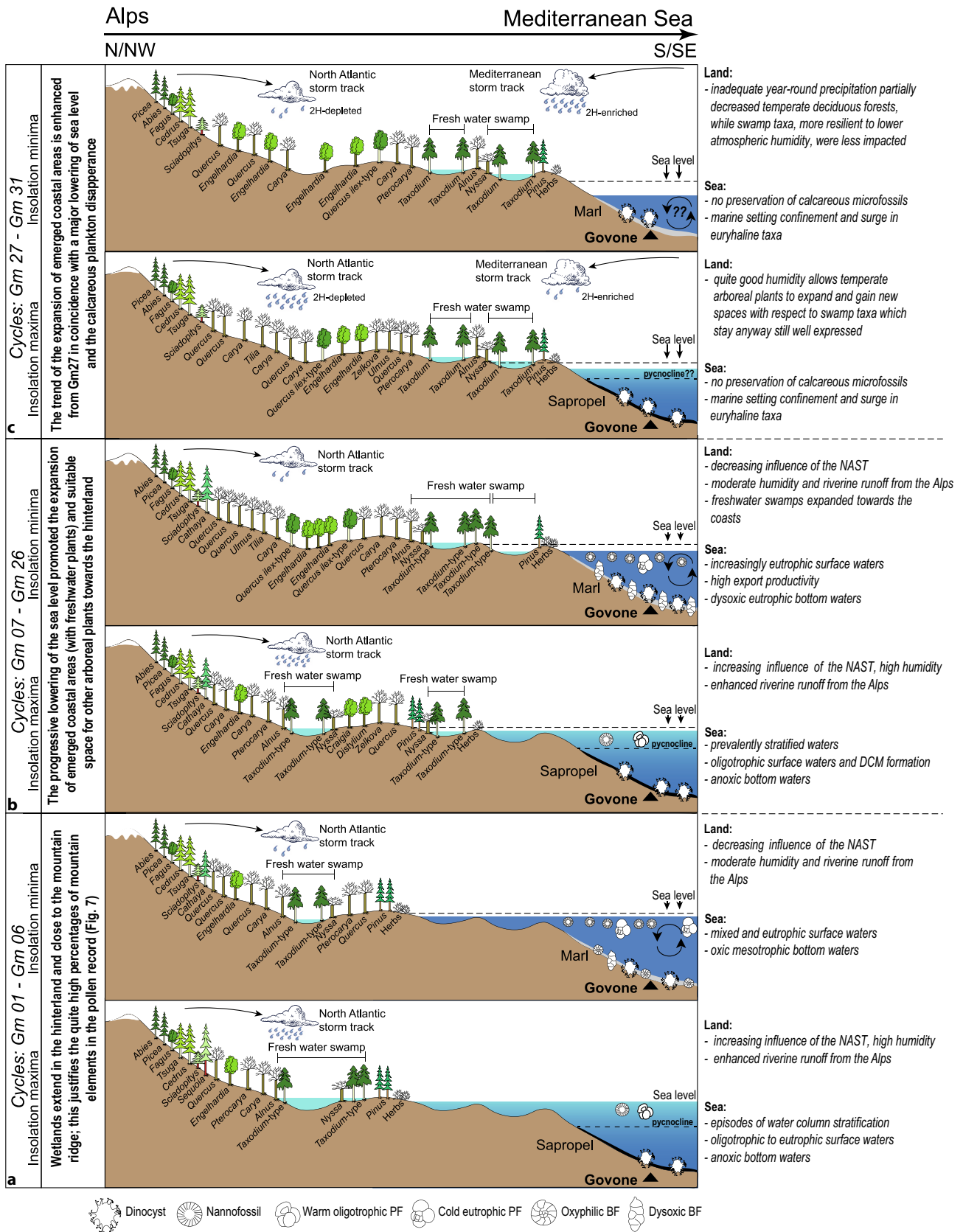


Fig. 9. Paleoenvironmental reconstructions of the Piedmont basin from 6.61 Ma (cycle Gm01) to 5.96 Ma (cycle Gm31). a) between 6.61 Ma and 6.515 Ma (Gm01 to Gm06); b) between 6.515 Ma and 6.075 Ma (Gm07 to Gm26), c) between 6.075 Ma and 5.945 Ma (Gm27 to Gm31). Paleoclimatic and paleohydrological reconstruction in c) is according to Sabino et al. (2020). NAST: North Atlantic Storm Track, DCM: Deep Chlorophyll Maximum; PF: Planktic Foraminifera, BF: Benthic Foraminifera.

the section possibly as a consequence of a taphonomic bias linked to the effect of the sea-level lowering (i.e. increase of distance between the mountain coniferous and the pollen depositional environment). Paleoenvironmental and paleoclimate conditions seem to have prevented the expansion of both freshwater and salt marshes despite the presence of some taxa, such as *Amaranthaceae* and *Poaceae*. This suggests areas with a very low herbaceous cover during both the pre-evaporitic Messinian and across the MSC onset. Such paleoclimatic reconstruction agrees with others independent datasets from leaf waxes-sourced molecular fossils (long chain *n*-alkanes; Natalicchio et al., 2019; Sabino et al., 2020, 2021a, 2021b). In particular, long chain *n*-alkane distribution pattern and their stable carbon isotope values support a C₃-dominated continental vegetation and rather humid climate during the earliest phase of the MSC in this northernmost edge of the Mediterranean basin.

According to palynological data, the broad-leaved evergreen-warm mixed forest is the solely biome attested to be present in the Piedmont basin, as well as in Northern Apennines sites (Bertini, 2006; Fauquette et al., 2006; Bertini and Menichetti, 2015). The xerophytic woods-shrub, or the warm grass-shrub biome have been largely documented solely in southern Mediterranean sites (Fauquette et al., 1999, 2006).

In summary, arid conditions apparently never developed in the Piedmont basin during the deposition of the pre-evaporitic sediments and across the MSC onset.

The two main vegetal patterns expressed by the expansion vs reduction of *Taxodioideae*, according to the precession-controlled sedimentary cyclicity (sapropel-marl couplets) pointed out prevalent (but not exclusive) alternations between warm and humid conditions (higher *Taxodioideae* values in sapropel) and less warm and less humid conditions (lower *Taxodioideae* values in marl) up to ca 6.02 Ma (Figs. 7, 9a, b), when an inversion in the patterns is evident (see in 5.3; Figs. 7, 9c). Throughout the pollen record the progressive increase of mesothermic trees withstanding a strong annual temperature cycle (with a cold winter season and a warm summer season), as well as the occurrence, though sporadic, of some taxa today typical of warm Mediterranean climates, suggest a quite good increase in seasonality. This behaviour is more evident from 6.2 to 6.1 Ma, possibly in connection with global climate changes (Herbert et al., 2016) and tectonically controlled, major shallowing of the Mediterranean gateway (e.g. Krijgsman et al., 2018).

5.3. Atmosphere and hydrographic changes across the onset of the MSC

In the late Miocene, shifts in the carbon cycle, involving a drawdown of atmospheric CO₂ and alterations in atmospheric circulation patterns, led to a cooling of the climate, heightened seasonality and aridity, along with concurrent changes to C₃ versus C₄ vegetation (Herbert et al., 2016). In the Piedmont basin (Northern Italy), the effects of these changes in the terrestrial environments and ecosystems do not include evidence of C₄ grasslands expansions at the expense of C₃-dominated ecosystems or marked increase of aridity as proposed for large areas of the tropics and subtropics (Ehleringer et al., 1997) and southern Mediterranean (Mayser et al., 2017; Butiseacă et al., 2021). Conversely, as discussed in 5.2., the forest and other wooded land stayed well expanded. The large and persistent presence of swamps, observed also in many other sites of the Mediterranean north of 42°N (e.g. Northern Apennines; Bertini and Menichetti, 2015), possibly played a non-negligible role in the global carbon cycle, acting both as sinks for carbon dioxide and as sources of methane (e.g.: Mitra et al., 2005; Tang et al., 2020; Hondula et al., 2021; Davidson et al., 2022). Today, wetlands are the largest natural source of methane (CH₄) releases in the global CH₄ budget, contributing for about one third to the total natural and anthropogenic emissions; however, wetland CH₄ feedbacks are not fully understood due to the paucity of data (e.g. Bloom et al., 2016; Shoemaker et al., 2021; Wang et al., 2021; Li et al., 2023). Palynological evidence would shed light on this issue by providing valuable

information over a very long interval of time (Keller, 2011; Beerling et al., 2009); especially relevant could be the reconstructions of changes in temperature values by climate quantification methods (e.g. Fauquette et al., 2006; Fauquette and Bertini, 2003). In the Mediterranean area, for example, *Taxodium/Glyptostrobus* swamps are documented, at least from the latest Tortonian to about 1.2 Ma (Calabrian) in coincidence with the disappearance of subtropical ecosystems from the Mediterranean area (Bertini and Martinetto, 2011; Combourieu-Nebout et al., 2015).

Today the climate variability in the Piedmont basin is the result of the effects of large-scale circulation. The North Atlantic Oscillation (NAO) affects winter climate, with positive phases of NAO leading to warm winters with reduced precipitation. On the other hands, the positive phases of Scandinavian - SCAN pattern led to increased precipitation, particularly in fall, and to a decrease in maximum temperatures. Consequently, frequent blocking episodes (Wazneh et al., 2021) over northern Europe promote both an increase of fall precipitation and colder temperatures. The northern Mediterranean area is also exposed to very humid flows from the Mediterranean Sea (Mediterranean storm track; Flaounas et al., 2022 and references therein). During the Messinian, the influence of the North Atlantic storm track (e.g. Kutzbach et al., 2014) and/or net convective precipitations over the Mediterranean Sea (Bosmans et al., 2015) possibly interacted with the main local source of freshwater transported by rivers draining the uplifted Alpine chain at insolation maxima, in phase with the African monsoon (Meijer and Tuenter, 2007; Toucanne et al., 2015). This resulted in the dominant pattern associated to sapropel/marl lithological cycles (Fig. 9a-c). At Govone, a cyclical enhanced contribution of moisture from the North Atlantic Storm track is revealed by hydrogen stable isotope composition of molecular fossils (long-chain *n*-alkanes) derived from plant-waxes during phases of insolation maxima (sapropel deposition) (Sabino et al., 2020) for the cycles deposited between 6.069 and ca 5.92 (Gm26 to Gm33) with the onset of the MSC between cycles Gm29 and Gm30 (Fig. 9c). Such dataset suggested a progressive increase of moisture from the evaporating Mediterranean Sea to the Piedmont basin during the first MSC phase, concomitantly with a reduction of the Atlantic-Mediterranean connection (e.g. Flecker et al., 2015).

The Govone pollen data confirm that deposition was controlled by precession-driven climate fluctuations with sapropels prevalently accumulated during warmer and more humid climate (at insolation maxima) conditions with respect to marls (at insolation minima), under the effects of global and regional factors (Figs. 7, 8, 9a-c). Sapropel deposition often corresponds with the timing of maxima of the Mediterranean autumn/winter storm track precipitation and the North African summer monsoon. Such conditions enhanced the expansion of swamp vegetal formations which on the contrary show, more often, some decrease during marls deposition (Fig. 9a, b). However, from ca 6.03 Ma (cycle Gm27), this dominant pattern in the sapropel/marl couplets was suddenly reversed during (at least) four, consecutive cycles, up to cycle Gm31 (5.962 Ma; topmost studied cycle; Fig. 9c); this interval includes the disappearance of calcareous microfossil and the onset of the MSC fixed in cycle Gm30 by Gennari et al. (2020) and Sabino et al. (2020). This apparent vegetational change in the uppermost part of the Govone record is not reflected by changes in the lithology of the cycles; however, such a pattern was also sporadically recorded in some of the older cycles (e.g. Gm04 and Gm14). To test whether such reversal of pollen percentages in the sapropel/marl couplets reflects a local to regional climate perturbation, a first comparison has been carried out with geochemical data from the same site (Sabino et al., 2020, 2021a). Unfortunately, the comparison was possible only from cycle Gm27 upwards, because of the absence of geochemical data for the underlying cycles. The geochemical dataset, including element/Al ratios and abundance of plant waxes-derived *n*-alkanes, agrees with humid conditions and an increased riverine runoff during sapropel deposition (insolation maxima) and less humid conditions during marls deposition (insolation minima) (Natalicchio et al., 2019; Sabino et al., 2020). Palynological data suggest the possibility that this inversion

pattern results from the combined influence of sea level oscillations and regional environmental/climate changes which superimposed to global factors.

As a summary, according to palynology during the deposition of cycles Gm01–Gm06 humidity was high at insolation maxima possibly because of the increasing influence of the North Atlantic Storm track, resulting in enhanced riverine runoff from the Alps and development of freshwater swamp areas (Fig. 9a). Both salt and freshwater marshes were not common portions of wetland ecosystems. The latter were close to the hinterland and mountain ridge, as attested by the quite high percentages of mountain elements in the pollen record. The progressive lowering of the sea level promoted the expansion of emerged coastal areas and suitable space for arboreal plants (cycles Gm07–26; Fig. 9b). This trend is enhanced at 6.033 Ma (from cycle Gm27), in coincidence with the disappearance of calcareous plankton (6.02 Ma), and a major lowering of sea level (Fig. 9c). Subtropical and temperate broad-leaved deciduous forests (especially swamp taxa) largely expanded in the new environment under the effect of local and global climate change. The progressive increase of temperate broad-leaved deciduous forests suggests a higher seasonality associated to the progressive closure of Atlantic-Mediterranean connections and lowering of sea level. The peculiar environmental and climate context may explain such reversal pattern of vegetal assemblages, during this transitional phase including the MSC onset (Figs. 8, 9c): i. during sapropel deposition, the quite good humidity allows temperate arboreal plants to expand and gain new spaces with respect to swamp taxa which stay anyway still well expressed; ii. during marl deposition relatively harsher conditions enhanced a partial decrease of the temperate broad-leaved deciduous forests (inadequate precipitation in all months) whereas swamp taxa were not especially affected because of their ability to withstand phases of lower atmospheric humidity.

6. Conclusion

At Govone the set of biological evidence over the 31 sedimentary cycles permits to trace the contemporary changes in both terrestrial and marine environments in the Piedmont basin, one of the northernmost basins of the Mediterranean (44°N and 8°E), between 6.6 Ma, and 5.96 Ma just after the beginning of the MSC.

Marine proxies document, along with the overall progressive restriction of the Mediterranean, a sequence of minor, punctuated marine and freshwater influxes up to 6.02 Ma when inner neritic areas with lagoon settings, typified by frequent salinity fluctuations, expanded according to the organic-walled dinoflagellate cysts. At that time calcareous nannoplankton and foraminifers apparently disappear from the stratigraphical record, in dependence of the environmental changes and/or possibly taphonomic biases. According to the previous established chronostratigraphic frame, this disappearance predates of about 50 kyr the MSC onset which is marked by a good increase of the warm acritarch *Nannobarbophora*. The critical discussion on the timing of MSC onset as well as its synchronous versus diachronous nature are not within the scope of this work; however, the relevance of the detected ecological and climatic evidence associated to several high-resolution bio-events could represent a unique contribution for further chronostratigraphic and geochronological investigations.

On the land, at least since 6.6 Ma, arid conditions, typical of southern areas, especially to be expected during precession maxima or glacials, have not been detected at these latitudes where, on the contrary, prevalent humid conditions are attested by a dominant arboreal vegetation, including taxa typical of freshwater swamps, before and across the MSC onset. The overall vegetal pattern, associated to the presence of the broad-leaved evergreen-warm mixed forest biome, confirms the occurrence of marked climate gradients within the Mediterranean area, when compared to the dominant occurrence of xerophytic woods-scrub/warm grass-shrub biomes in the southern region. The progressive increase of seasonality with changes in time and amount of precipitation during the

year, parallels the ongoing isolation of the Mediterranean Sea from the Atlantic Ocean. The role of the close Alpine region (high altitude), along with regional runoff inputs, is especially enhanced and crucial at this point of the history, close to the beginning of the MSC.

Supplementary data to this article can be found online at <https://doi.org/10.1016/j.gloplacha.2024.104362>.

CRediT authorship contribution statement

Adele Bertini: Conceptualization, Data curation, Funding acquisition, Investigation, Methodology, Project administration, Resources, Supervision, Validation, Visualization, Writing – original draft, Writing – review & editing. **Gabriele Niccolini:** Conceptualization, Data curation, Formal analysis, Investigation, Methodology, Writing – original draft, Writing – review & editing. **Rocco Gennari:** Conceptualization, Data curation, Writing – original draft, Writing – review & editing. **Francesca Lozar:** Data curation, Formal analysis, Investigation, Methodology, Resources, Writing – original draft, Writing – review & editing, Funding acquisition. **Elena Menichetti:** Investigation, Methodology, Writing – review & editing. **Marcello Natalicchio:** Resources, Writing – review & editing, Funding acquisition. **Francesco Dela Pierre:** Funding acquisition, Project administration, Resources, Writing – review & editing, Supervision.

Declaration of competing interest

The authors declare the following financial interests/personal relationships which may be considered as potential competing interests.

Adele Bertini reports financial support was provided by University of Firenze. Gabriele Niccolini reports financial support was provided by University of Firenze, Department of Earth Sciences. Rocco Gennari reports financial support was provided by University of Torino, Department of Earth Science. Francesca Lozar reports financial support was provided by University of Torino, Department of Earth Science. Francesco dela Pierre reports was provided by University of Torino, Department of Earth Science. Marcello Natalicchio reports was provided by University of Torino, Department of Earth Science. Elena Menichetti reports was provided by University of Firenze, Department of Earth Sciences.

Data availability

We have shared data in the Supplementary Material.

Acknowledgements

We thank the Editor, H. Corbi, and an anonymous reviewer for their very constructive comments, which helped to improve the manuscript.

References

- Artoni, A., Papani, G., Rizzini, F., Calderoni, M., Bernini, M., Argnani, A., Roveri, M., Rossi, M., Rogledi, S., Gennari, R., 2004. The Salsomaggiore structure (Northwestern Apennine foothills, Italy): a Messinian mountain front shaped by mass-wasting products. *Geoacta* 3, 107–128.
- Bahr, A., Kaboth-Bahr, S., Karas, C., 2022. The opening and closure of oceanic seaways during the Cenozoic: pacemaker of global climate change? *Geol. Soc. Spec. Publ.* 523 (1), 523–2021. <https://doi.org/10.1144/SP523-2021-54>.
- Bartol, M., Pavšič, J., Dobnikar, M., Bernasconi, S.M., 2008. Unusual *Braarudosphaera bigelowii* and *Micrantholithus vesper* enrichment in the early Miocene sediments from the Slovenian Corridor, a seaway linking the Central Paratethys and the Mediterranean. *Palaeogeogr. Palaeoclimatol. Palaeoecol.* 267, 77–88. <https://doi.org/10.1016/j.palaeo.2008.06.005>.
- Baumann, K.H., Saavedra-Pellitero, M., Böckel, B., Ott, C., 2016. Morphometry, biogeography and ecology of *Calcidiscus* and *Umbilicosphaera* in the South Atlantic. *Rev. Micropaleontol.* 59 (3), 239–251. <https://doi.org/10.1016/j.revmic.2016.03.001>.
- Beerling, D., Berner, R.A., Mackenzie, F.T., Harfoot, M.B., Pyle, J.A., 2009. Methane and the CH₄ related greenhouse effect over the past 400 million years. *Am. J. Plant Sci.* 309 (2), 97–113. <https://doi.org/10.2475/02.2009.01>.

- Berger, A., Loutre, M.F., 2010. Modelling the 100-kyr glacial–interglacial cycles. *Glob. Planet. Chang.* 72 (4), 275–281. <https://doi.org/10.1016/j.gloplacha.2010.01.003>.
- Bertini, A., 2006. The Northern Apennines palynological record as a contribute for the reconstruction of the Messinian palaeoenvironments. *Sediment. Geol.* 188–189, 235–258. <https://doi.org/10.1016/j.sedgeo.2006.03.007>.
- Bertini, A., Combourieu-Nebout, N., 2023. Piacenzian to late Pleistocene flora and vegetation in Italy: a moving sketch. *Alp. Mediterr. Quat.* 36 (1), 91–119. <https://doi.org/10.26382/AMQ.2023.05>.
- Bertini, A., Martinetto, E., 2008. Messinian to Zanclean vegetation and climate of Northern and Central Italy. *Boll. Soc. Pal. It.* 47 (2), 105–121.
- Bertini, A., Martinetto, E., 2011. Reconstruction of vegetation transects for the Messinian-Piacenzian of Italy by means of comparative analysis of pollen, leaf and carpological records. *Palaeogeogr. Palaeoclimatol. Palaeoecol.* 304, 230–246. <https://doi.org/10.1016/j.palaeo.2010.09.005>.
- Bertini, A., Menichetti, E., 2015. Palaeoclimate and palaeoenvironments in Central Mediterranean during the last 1.6 Ma before the onset of the Messinian Salinity Crisis: a case study from the Northern Apennine foredeep basin. *Rev. Palaeobot. Palynol.* 218, 106–116. <https://doi.org/10.1016/j.revpalbo.2014.08.011>.
- Bialik, O.M., Frank, M., Betzler, C., Zammit, R., Waldmann, N.D., 2019. Two-step closure of the Miocene Indian Ocean Gateway to the Mediterranean. *Sci. Rep.* 9 (1), 1–10. <https://doi.org/10.1038/s41598-019-45308-7>.
- Blanc-Valleron, M.M., Pierre, C., Caulet, J.P., Caruso, A., Rouchy, J.M., Cespuglio, G., Sprovieri, R., Pestrea, S., Di Stefano, S., 2002. Sedimentary, stable isotope and micropaleontological records of paleoceanographic change in the Messinian Tripoli Formation (Sicily, Italy). *Palaeogeogr. Palaeoclimatol. Palaeoecol.* 185 (3–4), 255–286. [https://doi.org/10.1016/S0031-0182\(02\)00302-4](https://doi.org/10.1016/S0031-0182(02)00302-4).
- Bloom, A.A., Lauvaux, T., Worden, J., Yadav, V., Duren, R., Sander, S.P., Schimel, D.S., 2016. What are the greenhouse gas observing system requirements for reducing fundamental biogeochemical process uncertainty? Amazon wetland CH₄ emissions as a case study. *Atmos. Chem. Phys.* 16 (23), 15199–15218. <https://doi.org/10.5194/acp-16-15199-2016>.
- Bonomo, S., Schroeder, K., Cascella, A., Alberico, I., Lirer, F., 2021. Living coccolithophore communities in the Central Mediterranean Sea (Summer 2016): Relations between ecology and oceanography. *Mar. Micropaleontol.* 165, 101995. <https://doi.org/10.1016/j.marmicro.2021.101995>.
- Bosmans, J.H.C., Drijfhout, S.S., Tuenter, E., Hilgen, F.J., Lourens, L.J., Rohling, E.J., 2015. Precession and obliquity forcing of the freshwater budget over the Mediterranean. *Quat. Sci. Rev.* 123, 16–30. <https://doi.org/10.1016/j.quascirev.2015.06.008>.
- Bown, P.R., Young, J.R., 1998. Techniques. In: Bown, P.R. (Ed.), *Calcareous Nannofossil Biostratigraphy*. Chapman and Hall, London, pp. 16–28.
- Brenner, W.W., 2001a. Distribution of organic walled microfossils within single lamina from the Gotland Basin, and their environmental evidence. *Baltica* 14, 34–39.
- Brenner, W.W., 2001b. Organic-walled microfossils from the Central Baltic Sea, indicators of environmental change and base for ecostratigraphic correlation. *Baltica* 14, 40–51.
- Brenner, W.W., 2005. Holocene environmental history of the Gotland Basin (Baltic Sea) — a micropaleontological model. *Palaeogeogr. Palaeoclimatol. Palaeoecol.* 220 (3–4), 227–241. <https://doi.org/10.1016/j.palaeo.2004.12.010>.
- Bukry, D., 1974. Coccoliths as paleosalinity indicators—evidence from the Black Sea. In: Degens, E.T., Ross, D.A. (Eds.), *The Black Sea—Geology, Chemistry, and Biology*, vol. 2. AAPG Mem, pp. 353–363.
- Butiseacă, G.A., Vasiliev, I., van der Meer, M.T.J., Krijgsman, W., Palcu, D.V., Feurdean, A., Niedermeyer, E.M., Mulch, A., 2021. Severe late Miocene droughts affected Eurasia. *Glob. Planet. Chang.* 206, 103644. <https://doi.org/10.1016/j.gloplacha.2021.103644>.
- Capella, W., Barhoun, N., Flecker, R., Hilgen, F.J., Kouwenhoven, T., Matenco, L.C., Sierro, F.J., Toubert, M.A., Yousfi, M.Z., Krijgsman, W., 2018. Palaeogeographic evolution of the late Miocene Rifian Corridor (Morocco): reconstructions from surface and subsurface data. *Earth Sci. Rev.* 180, 37–59. <https://doi.org/10.1016/j.earscirev.2018.02.017>.
- Capella, W., Flecker, R., Hernández-Molina, F.J., Simon, D., Meijer, P.T., Rogerson, M., Krijgsman, W., 2019. Mediterranean isolation preconditioning the Earth System for late Miocene climate cooling. *Sci. Rep.* 9 (1), 1–8. <https://doi.org/10.1038/s41598-019-40208-2>.
- Capella, W., Spakman, W., van Hinsbergen, D.J., Chertova, M.V., Krijgsman, W., 2020. Mantle resistance against Gibraltar slab dragging as a key cause of the Messinian Salinity Crisis. *Terra Nova* 32 (2), 141–150. <https://doi.org/10.1111/ter.12442>.
- Carminati, E., Doglioni, C., 2012. Alps vs. Apennines: the paradigm of a tectonically asymmetric Earth. *Earth Sci. Rev.* 112 (1–2), 67–96. <https://doi.org/10.1016/j.earscirev.2012.02.004>.
- Casas-Gallego, M., Lassaletta, L., Barrón, E., Bruch, A.A., Montoya, P., 2015. Vegetation and climate in the eastern Iberian Peninsula during the pre-evaporitic Messinian (late Miocene). Palynological data from the Upper Turolian of Venta del Moro (Spain). *Rev. Palaeobot. Palynol.* 215, 85–99. <https://doi.org/10.1016/j.revpalbo.2015.01.001>.
- Christensen, J.H., Carter, T.R., Rummukainen, M., Amanatidis, G., 2007. Evaluating the performance and utility of regional climate models: the PRUDENCE project. *Clim. Chang.* 81, 1–6.
- Collins, J.A., Schefuß, E., Mulitza, S., Prange, M., Werner, M., Tharammal, T., Paul, A., Wefer, G., 2013. Estimating the hydrogen isotopic composition of past precipitation using leaf-waxes from western Africa. *Quat. Sci. Rev.* 65, 88–101. <https://doi.org/10.1016/j.quascirev.2013.01.007>.
- Combourieu-Nebout, N., Bertini, A., Russo-Ermolli, E., Peyron, O., Klotz, S., Montade, V., Fauquette, S., Allen, J.R.M., Fusco, F., Goring, S., Huntley, B., Joannin, S., Lebreton, V., Magri, D., Martinetto, E., Orain, R., Sadori, L., 2015. Climate changes in the Central Mediterranean and Italian vegetation dynamics since the Pliocene. *Rev. Palaeobot. Palynol.* 218, 127–147. <https://doi.org/10.1016/j.revpalbo.2015.03.001>.
- Corbi, H., Soria, J.M., 2016. Late Miocene-early Pliocene planktonic foraminifer event-stratigraphy of the Bajo Segura basin: a complete record of the western Mediterranean. *Mar. Pet. Geol.* 77, 1010–1027. <https://doi.org/10.1016/j.marpetgeo.2016.08.004>.
- Corbi, H., Soria, J.M., Lancis, C., Giannetti, A., Tent-Manclús, J.E., Dinarès-Turell, J., 2016. Sedimentological and paleoenvironmental scenario before, during, and after the Messinian Salinity Crisis: the San Miguel de Salinas composite section (western Mediterranean). *Mar. Geol.* 379, 246–266. <https://doi.org/10.1016/j.margeo.2016.05.017>.
- Corbi, H., Soria, J.M., Giannetti, A., Yébenes, A., 2020. The step-by-step restriction of the Mediterranean (start, amplification, and consolidation phases) preceding the Messinian Salinity Crisis (climax phase) in the Bajo Segura basin. *Geo-Mar. Lett.* 40 (3), 341–361. <https://doi.org/10.1007/s00367-020-00647-7>.
- Cos, J., Doblas-Reyes, F., Jury, M., Marcos, R., Bretonnière, P.A., Samsó, M., 2022. The Mediterranean climate change hotspot in the CMIP5 and CMIP6 projections. *Earth Syst. Dynam.* 13 (1), 321–340. <https://doi.org/10.5194/esd-13-321-2022>.
- Dale, B., 1996. Dinoflagellate cyst ecology: Modeling and geological applications. In: Jansonius, J., McGregor, D.C. (Eds.), *Palynology: Principles and Applications*, vol. 3. American Association of Stratigraphic Palynologists Foundation, Dallas, pp. 1249–1275.
- Davidson, S.J., Dazé, E., Byun, E., Hiler, D., Kangur, M., Talbot, J., Finkelstein, S.A., Strack, M., 2022. The unrecognized importance of carbon stocks and fluxes from swamps in Canada and the USA. *Environ. Res. Lett.* 17 (5), 053003.
- De Vernal, A., Goyette, C., Rodrigues, C., 1989. Contribution palynostratigraphique (dinokystes, pollen et spores) à la connaissance de la mer de Champlain: coupe de Saint-Cézaire, Québec. *Can. J. Earth Sci.* 26, 2450–2464.
- Dela Pierre, F., Bernardi, E., Cavagna, S., Clari, P., Gennari, R., Irace, A., Lozar, F., Lugli, S., Manzi, V., Natalicchio, M., Roveri, M., Violanti, D., 2011. The record of the Messinian salinity crisis in the Tertiary Piedmont Basin (NW Italy): the Alba section revisited. *Palaeogeogr. Palaeoclimatol. Palaeoecol.* 310 (3–4), 238–255. <https://doi.org/10.1016/j.palaeo.2011.07.017>.
- Dela Pierre, F., Clari, P., Bernardi, E., Natalicchio, M., Costa, E., Cavagna, S., Lozar, F., Lugli, S., Manzi, V., Roveri, M., Violanti, D., 2012. Messinian carbonate-rich beds of the Tertiary Piedmont Basin (NW Italy): microbially-mediated products straddling the onset of the salinity crisis. *Palaeogeogr. Palaeoclimatol. Palaeoecol.* 344, 78–93. <https://doi.org/10.1016/j.palaeo.2012.05.022>.
- Dela Pierre, F., Natalicchio, M., Lozar, F., Bonetto, S., Carnevale, G., Cavagna, S., Colombero, S., Sabino, M., Violanti, D., 2016. The northernmost record of the Messinian salinity crisis (Piedmont basin, Italy). *Geol. F. Trips.* 8, 1–58. <https://doi.org/10.3301/GFT.2016.03>.
- Dimiza, M.D., Triantaphyllou, M.V., Malinverno, E., 2014. New evidence for the ecology of *Helicosphaera carteri* in polluted coastal environments (Elefsis Bay, Saronikos Gulf, Greece). *JNR* 34, 37–43.
- Drinia, H., Antonarakou, A., Tsaparas, N., Kontakiotis, G., 2007. Palaeoenvironmental conditions preceding the Messinian Salinity Crisis: a case study from Gavdos Island. *Geobios* 40 (3), 251–265. <https://doi.org/10.1016/j.geobios.2007.02.003>.
- Duarte-Silva, A., Palma, S., Sobrinho-Goncalves, L., Moita, M.T., 2004. *Braarudosphaera bigelowii* in waters of the upwelling coast of Portugal. *JNR* 26, 35.
- Ehleringer, J.R., Cerling, T.E., Helliker, B.R., 1997. C₄ photosynthesis, atmospheric CO₂, and climate. *Oecologia* 112 (3), 285–299.
- Ellegaard, M., 2000. Variations in dinoflagellate cyst morphology under conditions of changing salinity during the last 2000 years in the Limfjord, Denmark. *Rev. Palaeobot. Palynol.* 109 (1), 65–81. [https://doi.org/10.1016/S0034-6667\(99\)00045-7](https://doi.org/10.1016/S0034-6667(99)00045-7).
- Fauquette, S., Bertini, A., 2003. Quantification of the northern Italy Pliocene climate from pollen data: evidence for a very peculiar climate pattern. *Boreas* 32 (2), 361–369. <https://doi.org/10.1111/j.1502-3885.2003.tb01090.x>.
- Fauquette, S., Guiot, J., Suc, J.P., 1998a. A method for climatic reconstruction of the Mediterranean Pliocene using pollen data. *Palaeogeogr. Palaeoclimatol. Palaeoecol.* 144 (1–2), 183–201. [https://doi.org/10.1016/S0031-0182\(98\)00083-2](https://doi.org/10.1016/S0031-0182(98)00083-2).
- Fauquette, S., Quézel, P., Guiot, J., Suc, J.P., 1998b. Signification bioclimatique de taxons — guides du Pliocène Méditerranéen. *Geobios* 31, 151–169. [https://doi.org/10.1016/S0016-6995\(98\)80035-1](https://doi.org/10.1016/S0016-6995(98)80035-1).
- Fauquette, S., Suc, J.P., Guiot, J., Diniz, F., Feddi, N., Zheng, Z., Drivaliari, A., 1999. Climate and biomes in the West Mediterranean area during the Pliocene. *Palaeogeogr. Palaeoclimatol. Palaeoecol.* 152 (1–2), 15–36. [https://doi.org/10.1016/S0031-0182\(99\)00031-0](https://doi.org/10.1016/S0031-0182(99)00031-0).
- Fauquette, S., Suc, J.P., Bertini, A., Popescu, S.M., Wamy, S., Taoufiq, N.B., Perez Villa, M.J., Chikhi, H., Feddi, N., Subally, D., Clauzon, G., Ferrier, J., 2006. How did climate force the Messinian salinity crisis? Quantified climatic conditions from pollen records in the Mediterranean region. *Palaeogeogr. Palaeoclimatol. Palaeoecol.* 238 (1–4), 281–301. <https://doi.org/10.1016/j.palaeo.2006.03.029>.
- Fauquette, S., Suc, J.P., Jiménez-Moreno, G., Micheels, A., Jost, A., Favre, E., Bachiri Taoufiq, N., Bertini, A., Clet-Pellerin, M., Diniz, F., 2007. Latitudinal climatic gradients in the Western European and Mediterranean regions from the Mid-Miocene (c. 15 Ma) to the Mid-Pliocene (ca. 3.5 Ma) as quantified from pollen data. In: Williams, M., Haywood, A.M., Gregory, F.J., Schmidt, D.N. (Eds.), *Deep-Time Perspectives on Climate Change*. The Micropaleontological Society Special Publications. The Geological Society, London, pp. 481–502.
- Fauquette, S., Bertini, A., Manzi, V., Roveri, M., Argnani, A., Menichetti, E., 2015. Reconstruction of the Northern and Central Apennines (Italy) palaeoaltitudes during the late Neogene from pollen data. *Rev. Palaeobot. Palynol.* 218, 117–126. <https://doi.org/10.1016/j.revpalbo.2014.06.001>.

- Filippelli, G.M., Sierro, F.J., Flores, J.A., Vázquez, A., Utrilla, R., Pérez-Folgado, M., Latimer, J.C., 2003. A sediment-nutrient-oxygen feedback responsible for productivity variations in late Miocene sapropel sequences of the western Mediterranean. *Palaeogeogr. Palaeoclimatol. Palaeoecol.* 190, 335–348. [https://doi.org/10.1016/S0031-0182\(02\)00613-2](https://doi.org/10.1016/S0031-0182(02)00613-2).
- Flaounas, E., Davolio, S., Raveh-Rubin, S., Pantillon, F., Miglietta, M.M., Gaertner, M.A., Ricard, D., 2022. Mediterranean cyclones: current knowledge and open questions on dynamics, prediction, climatology and impacts. *Weather Clim. Dynam.* 3 (1), 173–208. <https://doi.org/10.5194/wcd-3-173-2022>.
- Flecker, R., Krijgsman, W., Capella, W., de Castro Martins, C., Dmitrieva, E., Mayser, J.P., Marzocchi, A., Modestu, S., Ochoa, D., Simon, D., Tulbure, M., van den Berg, B., van der Schee, M., de Lange, G., Ellam, R., Govers, R., Gutjahr, M., Hilgen, F., Kouwenhoven, T., Lofi, J., Meijer, P., Sierro, F.J., Bachiri, N., Barhoun, N., Alami, A. C., Chacon, B., Flores, J.A., Gregory, J., Howard, J., Lunt, D., Ochoa, M., Pancost, R., Vincent, S., Yousfi, M.Z., 2015. Evolution of the late Miocene Mediterranean-Atlantic gateways and their impact on regional and global environmental change. *Earth Sci. Rev.* 150, 365–392. <https://doi.org/10.1016/j.earscirev.2015.08.007>.
- Flores, J.A., Marino, M., Sierro, F.J., Hodell, D.A., Charles, C.D., 2003. Calcareous plankton dissolution pattern and coccolithophore assemblages during the last 600 kyr at ODP Site 1089 (Cape Basin, South Atlantic): paleoceanographic implications. *Palaeogeogr. Palaeoclimatol. Palaeoecol.* 196 (3–4), 409–426. [https://doi.org/10.1016/S0031-0182\(03\)00467-X](https://doi.org/10.1016/S0031-0182(03)00467-X).
- Flores, J.A., Sierro, F.J., Filippelli, G.M., Bárcena, M.A., Pérez-Folgado, M., Vázquez, A., Utrilla, R., 2005. Surface water dynamics and phytoplankton communities during deposition of cyclic late Messinian sapropel sequences in the western Mediterranean. *Mar. Micropaleontol.* 56, 50–79. <https://doi.org/10.1016/j.marmicro.2005.04.002>.
- Gennari, R., Manzi, V., Angeletti, L., Bertini, A., Biffi, U., Ceregato, A., Faranda, C., Gliozzi, E., Lugli, S., Menichetti, E., Rosso, A., Roveri, M., Taviani, M., 2013. A shallow water record of the onset of the Messinian salinity crisis in the Adriatic foredeep (Lagnagnone section, Northern Apennines). *Palaeogeogr. Palaeoclimatol. Palaeoecol.* 386, 145–164. <https://doi.org/10.1016/j.palaeo.2013.05.015>.
- Gennari, R., Lozar, F., Turco, E., Dela Pierre, F., Manzi, V., Natalicchio, M., Lugli, S., Roveri, M., Schreiber, C., Taviani, M., 2018. Integrated stratigraphy and paleoceanographic evolution of the pre-evaporitic phase of the Messinian salinity crisis in the Eastern Mediterranean as recorded in the Tokhni section (Cyprus island). *Newsl. Stratigr.* 50, 1–23. <https://doi.org/10.1127/nos/2017/0350>.
- Gennari, R., Lozar, F., Natalicchio, M., Zanella, E., Carnevale, G., Dela Pierre, F., 2020. Chronology of the Messinian events in the northernmost part of the Mediterranean: the Govone section (Piedmont Basin, NW Italy). *Riv. Ital. Paleontol. Stratigr.* 126, 517–560. <https://doi.org/10.13130/2039-4942/13705>.
- Gennari, R., Lugli, S., Manzi, V., Persico, D., Reghizzi, M., Roveri, M., 2024. Stress precursors of the Messinian salinity crisis as recorded by calcareous plankton and geochemistry in the Eastern Mediterranean: the Upper Metochia section of the Gavdos Island (Greece). *Palaeogeogr. Palaeoclimatol. Palaeoecol.* 636, 111970. <https://doi.org/10.1016/j.palaeo.2023.111970>.
- Giorgi, F., 2006. Climate change hot-spots. *Geophys. Res. Lett.* 33 (8), L08707. <https://doi.org/10.1029/2006GL025734>.
- Giorgi, F., Lionello, P., 2008. Climate change projections for the Mediterranean region. *Glob. Planet. Chang.* 63 (2–3), 90–104. <https://doi.org/10.1016/j.gloplacha.2007.09.005>.
- Gladstone, R., Flecker, R., Valdes, P., Lunt, D., Marwick, P., 2007. The Mediterranean hydrologic budget from a late Miocene global climate simulation. *Palaeogeogr. Palaeoclimatol. Palaeoecol.* 251, 254–267. <https://doi.org/10.1016/j.palaeo.2007.03.050>.
- Gualdi, S., Somot, S., May, W., Castellari, S., Déqué, M., Adani, M., Artale, V., Bellucci, A., Breitgang, J.S., Carrillo, A., Cornes, R., Dell’Aquila, A., Dubois, C., Efthymiadis, D., Elizalde, A., Gimeno, L., Godess, C.M., Harzallah, A., Krichak, S.O., Kuglitsch, F.G., Leckebusch, G.C., L’Hévéder, B., Li, L., Lionello, P., Luterbacher, J., Mariotti, A., Navarra, A., Nieto, R., Nissen, K.M., Oddo, P., Ruti, P., Sanna, A., Sannino, G., Scoccimarro, E., Sevault, F., Struglia, M.V., Toreti, A., Ulbrich, U., Xoplaki, E., 2013. Future climate projections. In: Navarra, A., Tubiana, L. (Eds.), *Regional Assessment of Climate Change in the Mediterranean*. Springer, Dordrecht, pp. 53–118.
- Hagino, K., Tomioka, N., Young, J.R., Takano, Y., Onuma, R., Horiguchi, T., 2016. Extracellular calcification of *Braarudosphaera bigelowii* deduced from electron microscopic observations of cell surface structure and elemental composition of pentoliths. *Mar. Micropaleontol.* 125, 85–94. <https://doi.org/10.1016/j.marmicro.2016.04.002>.
- Hagino, K., Tomioka, N., Tomioka, N., 2019. Seasonal succession of living coccolithophores in the coastal waters of Tomari Port. In: Jordan, R.W. (Ed.), *Coastal Coccolithophores*, vol. 4. JNR, Special Issue, Tottori, Japan, pp. 1–15.
- Harland, R., 1983. Distribution maps of recent dinoflagellate cysts in bottom sediments from the North-Atlantic Ocean and adjacent seas. *Palaeontology* 26, 321–387.
- Head, M.J., 2003. Neogene occurrences of the marine acritarch genus *Nannobarbophora* Habib and Knapp, 1982 emend., and the new species *N. Gedlii*. *J. Paleontol.* 77 (2), 382–385.
- Herbert, T.D., Lawrence, K.T., Tzanova, A., Peterson, L.C., Caballero-Gill, R., Kelly, C.S., 2016. Late Miocene global cooling and the rise of modern ecosystems. *Nat. Geosci.* 9 (11), 843. <https://doi.org/10.1038/ngeo2813>.
- Hilgen, F.J., Krijgsman, W., 1999. Cyclostratigraphy and astrochronology of the Tripoli diatomite formation (pre-evaporite Messinian, Sicily, Italy). *Terra Nova* 11, 16–22. <https://doi.org/10.1046/j.1365-3121.1999.00221.x>.
- Hilgen, F.J., Krijgsman, W., Langereis, C.G., Lourens, L.J., Santarelli, A., Zachariasse, W. J., 1995. Extending the astronomical (polarity) time scale into the Miocene. *Earth Planet. Sci. Lett.* 136, 495–510. [https://doi.org/10.1016/0012-821X\(95\)00207-S](https://doi.org/10.1016/0012-821X(95)00207-S).
- Hilgen, F.J., Aziz, H.A., Krijgsman, W., Raffi, I., Turco, E., 2003. Integrated stratigraphy and astronomical tuning of the Serravallian and lower Tortonian at Monte Dei Corvi (Middle-Upper Miocene, northern Italy). *Palaeogeogr. Palaeoclimatol. Palaeoecol.* 199, 229–264. [https://doi.org/10.1016/S0031-0182\(03\)00505-4](https://doi.org/10.1016/S0031-0182(03)00505-4).
- Hodell, D.A., Curtis, J.H., Sierro, F.J., Raymo, M.E., 2001. Correlation of late Miocene to early Pliocene sequences between the Mediterranean and North Atlantic. *Paleoceanography* 16 (2), 164–178. <https://doi.org/10.1029/1999PA000487>.
- Holbourn, A., Kuhnt, W., Frank, M., Haley, B.A., 2013. Changes in Pacific Ocean circulation following the Miocene onset of permanent Antarctic ice cover. *Earth Planet. Sci. Lett.* 365, 38–50. <https://doi.org/10.1016/j.epsl.2013.01.020>.
- Holbourn, A.E., Kuhnt, W., Clemens, S.C., Kochhann, K.G., Jöhneck, J., Lübbbers, J., Andersen, N., 2018. Late Miocene climate cooling and intensification of southeast Asian winter monsoon. *Nat. Commun.* 9 (1), 1584. <https://doi.org/10.1038/s41467-018-03950-1>.
- Hondula, K.L., Jones, C.N., Palmer, M.A., 2021. Effects of seasonal inundation on methane fluxes from forested freshwater wetlands. *Environ. Res. Lett.* 16 (8), 084016.
- Hüsing, S.K., Kuiper, K.F., Link, W., Hilgen, F.J., Krijgsman, W., 2009. The upper Tortonian–lower Messinian at Monte Dei Corvi (Northern Apennines, Italy): completing a Mediterranean reference section for the Tortonian stage. *Earth Planet. Sci. Lett.* 282 (1), 140–157. <https://doi.org/10.1016/j.epsl.2009.03.010>.
- Ijiri, A., Wang, L., Oba, T., Kawahata, H., Huang, C.Y., Huang, C.Y., 2005. Paleoenvironmental changes in the northern area of the East China Sea during the past 42,000 years. *Palaeogeogr. Palaeoclimatol. Palaeoecol.* 219 (3–4), 239–261. <https://doi.org/10.1016/j.palaeo.2004.12.028>.
- Jiménez-Moreno, G., Fauquette, S., Suc, J.P., 2010. Miocene to Pliocene vegetation reconstruction and climate estimates in the Iberian Peninsula from pollen data. *Rev. Palaeobot. Palynol.* 162, 403–415. <https://doi.org/10.1016/j.revpalbo.2009.08.001>.
- Jiménez-Moreno, G., Pérez-Asensio, J.N., Larrasoana, J.C., Aguirre, J., Civis, J., Rivas Carballo, M.R., Valle-Hernández, M.F., González-Delgado, J.A., 2013. Vegetation, sea-level, and climate changes during the Messinian salinity crisis. *Bull. Geol. Soc. Am.* 125, 432–444. <https://doi.org/10.1130/B30663.1>.
- Jones, H.L., Scrobola, Z., Bralower, T.J., 2021. Size and shape variation in the calcareous nannoplankton genus *Braarudosphaera* following the Cretaceous/Paleogene (K/Pg) mass extinction: clues as to its evolutionary success. *Paleobiology* 47 (4), 680–703.
- Keller, J.K., 2011. Wetlands and the global carbon cycle: what might the simulated past tell us about the future? *New Phytol.* 192 (4), 789–792. <https://doi.org/10.1111/j.1469-8137.2011.03954.x>.
- Kontakiotis, G., Butiseacă, G.A., Karakitsios, V., Antonarakou, A., Zarkogiannis, S., Agiadi, K., Krsnik, E., Besiou, E., Zachariasse, J.W., Lourens, L., Thivaiou, D., Koskeridou, E., Moissette, P., Mulch, A., Vasiliu, I., 2022. Hypersalinity accompanies tectonic restriction in the eastern Mediterranean prior to the Messinian Salinity Crisis. *Palaeogeogr. Palaeoclimatol. Palaeoecol.* 592 (2), 110903, 1014. <https://doi.org/10.1016/j.palaeo.2022.110903>.
- Kouwenhoven, T.J., van der Zwaan, G.J., 2006. A reconstruction of late Miocene Mediterranean circulation patterns using benthic foraminifera. *Palaeogeogr. Palaeoclimatol. Palaeoecol.* 238 (1), 373–385. <https://doi.org/10.1016/j.palaeo.2006.03.035>.
- Kouwenhoven, T.J., Hilgen, F.J., van der Zwaan, G.J., 2003. Late Tortonian-early Messinian stepwise disruption of the Mediterranean-Atlantic connections: constraints from benthic foraminiferal and geochemical data. *Palaeogeogr. Palaeoclimatol. Palaeoecol.* 198, 303–319. [https://doi.org/10.1016/S0031-0182\(03\)00472-3](https://doi.org/10.1016/S0031-0182(03)00472-3).
- Kouwenhoven, T.J., Morigi, C., Negri, A., Giunta, S., Krijgsman, W., Rouchy, J.M., 2006. Paleoenvironmental evolution of the eastern Mediterranean during the Messinian: Constraints from integrated microfossil data of the Pissouri Basin (Cyprus). *Mar. Micropaleontol.* 60, 17–44. <https://doi.org/10.1016/j.marmicro.2006.02.005>.
- Krijgsman, W., Hilgen, F.J., Raffi, I., Sierro, F.J., Wilson, D.S., 1999. Chronology, causes, progression of the Messinian salinity crisis. *Nature* 400, 652–655. <https://doi.org/10.1038/23231>.
- Krijgsman, W., Fortuin, A.R., Hilgen, F.J., Sierro, F.J., 2001. Astrochronology for the Messinian Sorbas basin (SE Spain) and orbital (precessional) forcing for evaporite cyclicity. *Sediment. Geol.* 140, 43–60. [https://doi.org/10.1016/S0037-0738\(00\)00171-8](https://doi.org/10.1016/S0037-0738(00)00171-8).
- Krijgsman, W., Blanc-Valleron, M.M., Flecker, R., Hilgen, F.J., Kouwenhoven, T.J., Merle, D., Orszag-Sperber, F., Rouchy, J.M., 2002. The onset of the Messinian salinity crisis in the Eastern Mediterranean (Pissouri Basin, Cyprus). *Earth Planet. Sci. Lett.* 194 (3–4), 299–310. [https://doi.org/10.1016/S0012-821X\(01\)00574-X](https://doi.org/10.1016/S0012-821X(01)00574-X).
- Krijgsman, W., Gabori, S., Hilgen, F., Iaccarino, S., Kaenel, E.D., Laan, E.V.D., 2004. Revised astrochronology for the Ain el Beida section (Atlantic Morocco): no glacio-eustatic control for the onset of the Messinian Salinity Crisis. *Stratigraphy* 1, 87–101.
- Krijgsman, W., Capella, W., Simon, D., Hilgen, F.J., Kouwenhoven, T.J., Meijer, P.T., Sierro, F.J., Tulbure, M.A., van den Berg, B.C.J., van der Schee, M., Flecker, R., 2018. The Gibraltar Corridor: watergate of the Messinian salinity crisis. *Mar. Geol.* 403, 238–246. <https://doi.org/10.1016/j.margeo.2018.06.008>.
- Krijgsman, W., Palcu, D.V., Andreetto, F., Stoica, M., Mandic, O., 2020. Changing seas in the late Miocene Northern Aegean: a Paratethyan approach to Mediterranean basin evolution. *Earth Sci. Rev.* 210, 103386. <https://doi.org/10.1016/j.earscirev.2020.103386>.
- Kroon, D., Wouters, P.F., Moodley, L., Ganssen, G., Troelstra, S.R., 1988. Phenotypic variation of *Turborotalita quinqueloba* (Natland) tests in living populations and in the Pleistocene of an Eastern Mediterranean piston core. In: Brummer, G.J.A., Kroon, D. (Eds.), *Planktonic Foraminifers as Tracers of Ocean–Climate History*. Free University Press, Amsterdam, pp. 131–147.

- Kutzbach, J.E., Chen, G., Cheng, H., Edwards, R.L., Liu, Z., 2014. Potential role of winter rainfall in explaining increased moisture in the Mediterranean and Middle East during periods of maximum orbitally-forced insolation seasonality. *Clim. Dyn.* 42, 1079–1095. <https://doi.org/10.1007/s00382-013-1692-1>.
- Larsen, H.C., Saunders, A.D., Clift, P.D., Beget, J., Wei, W., Spezzaferri, S., 1994. Seven million years of glaciation in Greenland. *Science* 264 (5161), 952–955.
- Laskar, J., Robutel, P., Joutel, F., Gastineau, M., Correia, A.C.M., Levrard, B., 2004. A long-term numerical solution for the insolation quantities of the Earth. *Astron. Astrophys.* 428, 261–285. <https://doi.org/10.1051/0004-6361:20041335>.
- Li, J., Pei, J., Fang, C., Li, B., Nie, M., 2023. Opposing seasonal temperature dependencies of CO₂ and CH₄ emissions from wetlands. *Glob. Chang. Biol.* 29, 1133–1143. <https://doi.org/10.1111/gcb.16528>.
- Lionello, P., Scarascia, L., 2018. The relation between climate change in the Mediterranean region and global warming. *Reg. Environ. Chang.* 18, 1481–1493. <https://doi.org/10.1007/s10113-018-1290-1>.
- Lionello, P., Scarascia, L., 2020. The relation of climate extremes with global warming in the Mediterranean region and its north versus south contrast. *Reg. Environ. Chang.* 20 (1), 31.
- Lionello, P., Malanotte-Rizzoli, P., Boscolo, R., Alpert, P., Artale, V., Li, L., Luterbacher, J., May, W., Trigo, R., Tsimplis, M., Ulbrich, U., Xoplaki, E., 2006. The Mediterranean climate: An overview of the main characteristics and issues. In: Lionello, P., Malanotte-Rizzoli, P., Boscolo, R. (Eds.), *Mediterranean Climate Variability*. Elsevier, Amsterdam, pp. 1–26. [https://doi.org/10.1016/S1571-9197\(06\)80003-0](https://doi.org/10.1016/S1571-9197(06)80003-0).
- Lionello, P., Abrantes, F., Congedi, L., Dulac, F., Gacic, M., Gomis, D., Goodess, C., Hoff, H., Kutie, L.H., Luterbacher, J., Planton, S., Reale, M., Schröder, K., Struglia, M. V., Toreti, A., Tsimplis, M., Ulbrich, U., Xoplaki, E., 2012. Introduction: Mediterranean climate: background information. In: Lionello, P. (Ed.), *The Climate of the Mediterranean Region. From the Past to the Future*. Elsevier, (NETHERLANDS), Amsterdam pp xxxv–xxxix, ISBN: 9780124160422.
- Lionello, P., Giorgi, F., Rohling, E., Seager, R., 2023. Mediterranean climate: Past, present and future. In: *Oceanography of the Mediterranean Sea*. Elsevier, pp. 41–91.
- Lirer, F., Foresi, L.M., Iaccarino, S.M., Salvatorini, G., Turco, E., Cosentino, C., Sierro, F. J., Caruso, A., 2019. Mediterranean Neogene planktonic foraminifer biozonation and biochronology. *Earth Sci. Rev.* 196, 102869 <https://doi.org/10.1016/j.earscirev.2019.05.013>.
- Lozar, F., Negri, A., 2019. A review of basin-wide calcareous nannofossil bioevents in the Mediterranean at the onset of the Messinian salinity crisis. *Mar. Micropaleontol.* 101752 <https://doi.org/10.1016/j.marmicro.2019.101752>.
- Lozar, F., Violanti, D., Bernardi, E., Dela Pierre, F., Natalicchio, M., 2018. Identifying the onset of the Messinian salinity crisis: a reassessment of the biochronostratigraphic tools (Piedmont Basin, NW Italy). *Newsl. Stratigr.* 51 (1), 11–31.
- Mancini, A.M., Gennari, R., Ziveri, P., Mortyn, P.G., Stolwijk, D.J., Lozar, F., 2020. Calcareous nannofossil and foraminiferal trace element records in the Sorbas Basin: a new piece of the Messinian Salinity Crisis onset puzzle. *Palaeogeogr. Palaeoclimatol. Palaeoecol.* 554, 109796.
- Mancini, A.M., Grelaud, M., Ziveri, P., Nallino, E., Lozar, F., 2021. Calcareous nannofossil size and abundance response to the Messinian Salinity Crisis onset and paleoenvironmental dynamics. *Palaeogeogr. Palaeoclimatol.* 36 (9) <https://doi.org/10.1029/2020PA004155> e2020PA004155.
- Mancini, A.M., Gennari, R., Natalicchio, M., Dela Pierre, F., Carnevale, G., Pastero, L., Pellegrino, L., Pilade, F., Lozar, F., 2022. Taphonomic bias on calcareous micro and nannofossils and paleoenvironmental evolution across the Messinian Salinity Crisis onset: Insights from the Sorbas Basin (SE Spain). *Palaeogeogr. Palaeoclimatol. Palaeoecol.* 111056 <https://doi.org/10.1016/j.palaeo.2022.111056>.
- Manzi, V., Roveri, M., Gennari, R., Bertini, A., Biffi, U., Giunta, S., Iaccarino, S.M., Lanci, L., Lugli, S., Negri, A., Riva, A., Rossi, M.E., Taviani, M., 2007. The deep-water counterpart of the Messinian lower Evaporites in the Apennine foredeep: the Fananello section (Northern Apennines, Italy). *Palaeogeogr. Palaeoclimatol. Palaeoecol.* 251, 470–499.
- Manzi, V., Lugli, S., Roveri, M., Schreiber, B.C., Gennari, R., 2011. The Messinian “Calcare di Base” (Sicily, Italy) revisited. *Geol. Soc. Am. Bull.* 123, 347–370.
- Manzi, V., Gennari, R., Hilgen, F., Krijgsman, W., Lugli, S., Roveri, M., Sierro, F.J., 2013. Age refinement of the Messinian salinity crisis onset in the Mediterranean. *Terra Nova* 25 (4), 1–8. <https://doi.org/10.1111/ter.12038>.
- Manzi, V., Gennari, R., Lugli, S., Minelli, N., Reghizzi, N., Roveri, M., Schreiber, B.C., 2016. Comment on “Carbonate deposition and diagenesis in evaporitic environments: the evaporative and Sulphur-bearing limestones during the settlement of the Messinian Salinity Crisis in Sicily and Calabria” by Caruso et al., 2015. *Palaeogeogr. Palaeoclimatol. Palaeoecol.* 429, 136–162. <https://doi.org/10.1016/j.palaeo.2015.08.011>.
- Manzi, V., Gennari, R., Lugli, S., Persico, D., Reghizzi, M., Roveri, M., Schreiber, B.C., Calvo, R., Gavrieli, I., Gvirtzman, Z., 2018. The onset of the Messinian Salinity Crisis in the deep Eastern Mediterranean basin. *Terra Nova* 30 (3), 189–198. <https://doi.org/10.1111/ter.12325>.
- Martinetto, E., Bertini, A., Mantzouka, D., Natalicchio, M., Niccolini, G., Kovar-Eder, J., 2022. Remains of a subtropical humid forest in a Messinian evaporite-bearing succession at Govone, northwestern Italy. *Foss. Impr.* 78 (1), 157–188. <https://doi.org/10.37520/fi.2022.007>.
- Mather, A., Martín, J.M., Harvey, A.M., Braga, J.C. (Eds.), 2001. *A Field Guide to the Neogene Sedimentary Basins of the Almería Province, South-East Spain*. Blackwell Science, Oxford, pp. 186–189.
- Matsuoka, K., 1987. Organic-walled dinoflagellate cysts from surface sediments of Akkeshi Bay and Lake Saroma, North Japan. *長崎大学教養部紀要. 自然科学篇* 28 (1), 35–123.
- Matthiessen, J., Brenner, W., 1996. Chlorococcalgalen und Dinoflagellaten-Zysten in rezenten Sedimenten des Greifswalder Bodden (südliche Ostsee). *Senckenberg. Marit.* 27 (1/2), 33–48.
- Maysers, J.P., Flecker, R., Marzocchi, A., Kouwenhoven, T.J., Lunt, D.J., Pancost, R.D., 2017. Precession driven changes in terrestrial organic matter input to the Eastern Mediterranean leading up to the Messinian Salinity Crisis. *Earth Planet. Sci. Lett.* 462, 199–211. <https://doi.org/10.1016/j.epsl.2017.01.029>.
- McMinn, A., 1991. Recent dinoflagellate cysts from estuaries on the central coast of New South Wales, Australia. *Micropaleontology* 269–287. <https://doi.org/10.2307/1485890>.
- Meijer, P.T., Tuenter, E., 2007. The effect of precession-induced changes in the Mediterranean freshwater budget on circulation at shallow and intermediate depth. *J. Mar. Syst.* 68, 349–365. <https://doi.org/10.1016/j.jmarsys.2007.01.006>.
- Miller, K.G., Mountain, G.S., Wright, J.D., Browning, J.V., 2011. A 180-million-year record of sea level and ice volume variations from continental margin and deep-sea isotopic records. *Oceanography* 24 (2), 40–53. <https://doi.org/10.5670/oceanog.2011.26>.
- Mitra, S., Wassmann, R., Vlek, P.L., 2005. An appraisal of global wetland area and its organic carbon stock. *Curr. Sci.* 88 (1), 25–35.
- Morigi, C., Negri, A., Giunta, S., Kouwenhoven, T., Krijgsman, W., Blanc-Valleron, M.M., Orszag-Sperber, F., Rouchy, J.M., 2007. Integrated quantitative biostratigraphy of the latest Tortonian-early Messinian Pissouri section (Cyprus): an evaluation of calcareous plankton bioevents. *Geobios* 40, 267–279. <https://doi.org/10.1016/j.geobios.2007.02.002>.
- Murray, J.W., 2006. *Ecology and Applications of Benthic Foraminifera*. Cambridge University Press, Cambridge.
- Natalicchio, M., Dela Pierre, F., Birgel, D., Brumsack, H., Carnevale, G., Gennari, R., Gier, S., Lozar, F., Pellegrino, L., Sabino, M., Schnetger, B., Peckmann, J., 2019. Paleoenvironmental change in a precession-paced succession across the onset of the Messinian salinity crisis: insight from element geochemistry and molecular fossils. *Palaeogeogr. Palaeoclimatol. Palaeoecol.* 518, 45–61. <https://doi.org/10.1016/j.palaeo.2019.01.009>.
- Natalicchio, M., Pellegrino, L., Clari, P., Pastero, L., Dela Pierre, F., 2021. Gypsum lithofacies and stratigraphic architecture of a Messinian marginal basin (Piedmont Basin, NW Italy). *Sediment. Geol.* 425, 106009 <https://doi.org/10.1016/j.sedgeo.2021.106009>.
- Nehring, S., 1994. Spatial distribution of dinoflagellate resting cysts in recent sediments of Kiel Bight, Germany (Baltic Sea). *Ophelia* 39 (2), 137–158. <https://doi.org/10.1080/00785326.1994.10429540>.
- Nehring, S., 1997. Dinoflagellate resting cysts from recent German coastal sediments. *Bot. Mar.* 40, 307–324.
- Niccolini, G., Martinetto, E., Lanini, B., Menichetti, E., Fusco, F., Hakobyan, E., Bertini, A., 2022. Late Messinian flora from the post-evaporitic deposits of the Piedmont Basin (Northwest Italy). *Foss. Impr.* 78 (1), 189–216. <https://doi.org/10.37520/fi.2022.008>.
- Nijenhuis, I.A., Schenau, S.J., Van der Weijden, C.H., Hilgen, F.J., Lourens, L.J., Zachariasse, W.J., 1996. On the origin of upper Miocene sapropelites. A case study from the Faneromeni section, Crete (Greece). *Paleoceanography* 11, 633–645. <https://doi.org/10.1029/96PA01963>.
- Okada, H., Honjo, S., 1973. The distribution of oceanic coccolithophorids in the Pacific. In: *Deep Sea Research and Oceanographic Abstracts*, 20(4), pp. 355–374.
- Peleo-Alampay, A.M., Mead, G.A., Wei, W., 1999. Unusual Oligocene *Braarudosphaera*-rich layers of the South Atlantic and their paleoceanographic implications. *JNR.* 21, 17–26.
- Pellegrino, L., Dela Pierre, F., Natalicchio, M., Carnevale, G., 2018. The Messinian diatomite deposition in the Mediterranean region and its relationships to the global silica cycle. *Earth Sci. Rev.* 178, 154–176. <https://doi.org/10.1016/j.earscirev.2018.01.018>.
- Pellegrino, L., Abe, K., Gennari, R., Lozar, F., Dela Pierre, F., Natalicchio, M., Mikami, Y., Jordan, R.W., Carnevale, G., 2020a. Integrated micropaleontological study of the Messinian diatomaceous deposits of the Monferrato Arc (Piedmont basin, NW Italy): new insights into the paleoceanographic evolution of the northernmost Mediterranean region. *Mar. Micropaleontol.* 160, 101910.
- Pellegrino, L., Dela Pierre, F., Jordan, R.W., Abe, K., Mikami, Y., Natalicchio, M., Gennari, R., Lozar, F., Carnevale, G., 2020b. The upper Miocene diatomaceous sediments of the northernmost Mediterranean region: a lamina-scale investigation of an overlooked paleoceanographic archive. *Sedimentology* 67, 3389–3421.
- Planton, S., Lionello, P., Artale, V., Aznar, R., Carrillo, A., Colin, J., Congedi, L., Dubois, C., Elizalde, A., Gualdif, S., Hertig, E., Jacobeit, J., Jordà, G., Li, L., Mariotti, A., Piani Ruti, C.P., Sanchez-Gomez, E., Sannino, G., Sevault, F., Somot, S., Tsimplis, M., 2012. The climate of the Mediterranean region in future climate projections. In: *The Climate of the Mediterranean Region*, 2012. Elsevier, Oxford, pp. 449–502. <https://doi.org/10.1016/B978-0-12-416042-2.00008-2>.
- Pospelova, V., Chmura, G.L., Boothman, W.S., Latimer, J.S., 2005. Spatial distribution of modern dinoflagellate cysts in polluted estuarine sediments from Buzzards Bay (Massachusetts, USA) embayments. *Mar. Ecol. Prog. Ser.* 292, 23–40.
- Prentice, I.C., Cramer, W., Harrison, S.P., Leemans, R., Monserud, R.A., Solomon, A.M., 1992. Special paper: a global biome model based on plant physiology and dominance, soil properties and climate. *J. Biogeogr.* 117–134 <https://doi.org/10.2307/2845499>.
- Raffi, I., Mozzato, C.A., Fornaciari, E., Hilgen, F.J., Rio, D., 2003. Late Miocene calcareous nannofossil biostratigraphy and astrochronology for the Mediterranean region. *Micropaleontology* 49, 1–26.
- Reille, M., 1992. Pollen et spores d'Europe et d'Afrique du Nord, vol. 1. *Laboratoire de Botanique historique et Palynologie*, Marseille.

- Rohling, E.J., Marino, G., Grant, K.M., 2015. Mediterranean climate and oceanography and the periodic development of anoxic events (sapropels). *Earth Sci. Rev.* 143, 62–97. <https://doi.org/10.1016/j.earscirev.2015.01.008>.
- Rouchy, J.M., Caruso, A., 2006. The Messinian salinity crisis in the Mediterranean basin: a reassessment of the data and an integrated scenario. *Sediment. Geol.* 188, 35–67.
- Roveri, M., Flecker, R., Krijgsman, W., Lofi, J., Lugli, S., Manzi, V., Sierro, F.J., Bertini, A., Camerlenghi, A., De Lange, G., Govers, R., Hilgen, F.J., Hübscher, C., Meijer, P.T., Stoica, M., 2014. The Messinian Salinity Crisis: past and future of a great challenge for marine sciences. *Mar. Geol.* 352, 25–58. <https://doi.org/10.1016/j.margeo.2014.02.002>.
- Sabino, M., Schefuß, E., Natalicchio, M., Dela Pierre, F., Birgel, D., Bortels, D., Schnetger, B., Peckmann, J., 2020. Climate and hydrologic variability in the northern Mediterranean across the onset of the Messinian salinity crisis. *Palaeogeogr. Palaeoclimatol. Palaeoecol.* 545, 109632 <https://doi.org/10.1016/j.palaeo.2020.109632>.
- Sabino, M., Dela Pierre, F., Natalicchio, M., Birgel, D., Gier, S., Peckmann, J., 2021a. The response of water column and sedimentary environments to the advent of the Messinian salinity crisis: insights from an onshore deep-water section (Govone, NW Italy). *Geol. Mag.* 158 (5), 825–841. <https://doi.org/10.1017/S0016756820000874>.
- Sabino, M., Birgel, D., Natalicchio, M., Dela Pierre, F., Peckmann, J., 2021b. Carbon isotope excursions during the late Miocene recorded by lipids of marine *Thaumarchaeota*, Piedmont Basin, Mediterranean Sea. *Geology* 50, 32–36. <https://doi.org/10.1130/G49342.1>.
- Sarmiento, J.L., Gruber, N., 2006. *Ocean Biogeochemical Dynamics*. Princeton University Press, Princeton.
- Schenu, S.J., Antonarakou, A., Hilgen, F.J., Lourens, L.J., Nijenhuis, I.A., van der Weijden, C.H., Zachariasse, W.J., 1999. Organic-rich layers in the Metochia section (Gavdos, Greece): evidence for a single mechanism of sapropel formation during the past 10 my. *Mar. Geol.* 153, 117–135. [https://doi.org/10.1016/S0025-3227\(98\)00086-3](https://doi.org/10.1016/S0025-3227(98)00086-3).
- Schiebel, R., Hemleben, C., 2017. *Planktic Foraminifers in the Modern Ocean*. Springer, Berlin, pp. 1–358.
- Shackleton, N.J., Backman, J., Zimmerman, H.T., Kent, D.V., Hall, M.A., Roberts, D.G., Schnitker, D., Baldauf, J.G., Desprairies, A., Homrighausen, R., Huddleston, P., Keene, J.B., Kaltenback, A.J., Krumsiek, K.A.O., Morton, A.C., Murray, J.W., Westberg-Smith, J., 1984. Oxygen isotope calibration of the onset of ice-rafting and history of glaciation in the North Atlantic region. *Nature* 307 (5952), 620–623.
- Shevenell, A.E., Kennett, J.P., Lea, D.W., 2008. Middle Miocene ice sheet dynamics, deep sea temperatures, and carbon cycling: a Southern Ocean perspective. *Geochem. Geophys. Geosyst.* 9, Q02006.
- Shoemaker, W.B., Anderson, F.E., Sirianni, M.J., Daniels, A., 2021. Carbon fluxes and potential soil accumulation within Greater Everglades cypress and pine forested wetlands. *Wetl. Ecol. Manag.* 371–384 <https://doi.org/10.1002/9781119639305.ch20>.
- Sierro, F.J., Hilgen, F.J., Krijgsman, W., Flores, J.A., 2001. The Abad composite (SE Spain): a Messinian reference section for the Mediterranean and the APTS. *Palaeogeogr. Palaeoclimatol. Palaeoecol.* 168 (1), 141–169. [https://doi.org/10.1016/S0031-0182\(00\)00253-4](https://doi.org/10.1016/S0031-0182(00)00253-4).
- Sierro, F.J., Flores, J.A., Francés, G., Vazquez, A., Utrilla, R., Zamarreño, I., Erlenkeuser, H., Barcena, M.A., 2003. Orbitally-controlled oscillations in planktic communities and cyclic changes in western Mediterranean hydrography during the Messinian. *Palaeogeogr. Palaeoclimatol. Palaeoecol.* 190, 289–316. [https://doi.org/10.1016/S0031-0182\(02\)00611-9](https://doi.org/10.1016/S0031-0182(02)00611-9).
- Simon, D., Marzocchi, A., Flecker, R., Lunt, D.J., Hilgen, F.J., Meijer, P.Th., 2017. Quantifying the Mediterranean freshwater budget throughout the late Miocene: new implications for sapropel formation and the Messinian salinity crisis. *Earth Planet. Sci. Lett.* 472, 25–37. <https://doi.org/10.1016/j.epsl.2017.05.013>.
- Stoica, M., Lazăr, I., Krijgsman, W., Vasiliev, I., Jipa, D., Floroiu, A., 2013. Paleoenvironmental evolution of the East Carpathian foredeep during the late Miocene-early Pliocene (Dacian Basin; Romania). *Glob. Planet. Chang.* 103, 135–148. <https://doi.org/10.1016/j.gloplacha.2012.04.004>.
- Suc, J.P., Bessais, E., 1990. Périennité d'un climat thermo-xérique en Sicile avant, pendant, après la crise de salinité messinienne. *Comptes rendus l'Académie des Sci. Série 2, Mécanique. Phys. Chim. Sci. l'univers. Sci. la Terre* 310, 1701–1707.
- Suc, J.P., Violanti, D., Londeix, L., Poumot, C., Robert, C., Clauzon, G., Gautier, F., Turon, J.L., Ferrier, J., Chikhi, H., Cambon, G., 1995. Evolution of the Messinian Mediterranean environments: the Tripoli Formation at Capodarso (Sicily, Italy). *Rev. Palaeobot. Palynol.* 87 (1), 51–79.
- Suc, J.P., Popescu, S.M., Fauquette, S., Bessedik, M., Jiménez Moreno, G., Bachiri Taoufik, N., Zheng, Z., Medail, F., Klotz, S., 2018. Reconstruction of Mediterranean flora, vegetation and climate for the last 23 million years based on an extensive pollen dataset. *Ecol. Mediterr.* 44 (2), 53–85.
- Tang, A.C., Melling, L., Stoy, P.C., Musin, K.K., Aeries, E.B., Waili, J.W., Shimizu, M., Poulter, B., Hirata, R., 2020. A Bornean peat swamp forest is a net source of carbon dioxide to the atmosphere. *Glob. Chang. Biol.* 26 (12), 6931–6944. <https://doi.org/10.1111/gcb.15332>.
- Thomsen, H.A., 2016. Baltic Sea coccolithophores—an overview of insights into their taxonomy and ecology from the last 40 years. *JNR* 36 (2), 97–119.
- Toucanne, S., Angue Minto'o, C.M., Fontanier, C., Bassetti, M.A., Jorry, S.J., Jouet, G., 2015. Tracking rainfall in the northern Mediterranean borderlands during sapropel deposition. *Quat. Sci. Rev.* 129, 178–195. <https://doi.org/10.1016/j.quascirev.2015.10.016>.
- Ulbrich, U., Xoplaki, E., Dobricic, S., García-Herrera, R., Lionello, P., Adani, M., Baldi, M., Barriopedro, D., Coccimiglio, P., Dalu, G., Efthymiadis, D., Gaetani, M., Galati, M.B., Gimeno, L., Goodess, C.M., Jones, P.D., Kuglitsch, F.G., Leckebusch, G.C., Luterbacher, J., Marcos-Moreno, M., Mariotti, A., Nieto, R., Nissen, K.M., Pettenuzzo, D., Pinaridi, N., Pino, C., Shaw, A.G.P., Sousa, P., Toreti, A., Trigo, R.M., Tsimplis, M., 2013. Past and current climate changes in the Mediterranean region. In: Navarra, A., Tubiana, L. (Eds.), *Regional Assessment of Climate Change in the Mediterranean*. Springer, Dordrecht, pp. 9–52. <https://doi.org/10.1175/2010JTECHO798.1>.
- van der Laan, E., Gaboardi, S., Hilgen, F.J., Lourens, L.J., 2005. Regional climate and glacial control on high-resolution oxygen isotope records from Ain El Beida (latest Miocene, NW Morocco): a cyclostratigraphic analysis in the depth and time domain. *Paleoceanography* 20, PA1001. <https://doi.org/10.1029/2003PA000995>.
- Vasiliev, I., Karakitsios, V., Bouloubassi, I., Agiadi, K., Kontakiotis, G., Antonarakou, A., Triantaphyllou, M., Gogou, A., Kafousia, N., de Rafélis, M., Zarkogiannis, S., Kaczmar, F., Parinos, C., Pasadakis, N., 2019. Large sea surface temperature, salinity, and productivity preservation changes preceding the onset of the Messinian Salinity Crisis in the eastern Mediterranean Sea. *Paleoceanogr. Paleoclimatol.* 34, 182–202. <https://doi.org/10.1029/2018PA003438>.
- Violanti, D., Lozar, F., Natalicchio, M., Dela Pierre, F., Bernardi, E., Clari, P., Cavagna, S., 2013. Stress-tolerant microfossils of a Messinian succession from the Northern Mediterranean basin (Pollenzo section, Piedmont, northwestern Italy). *Boll. Soc. Paleontol. Ital.* 52, 45–54.
- Wall, D., Dale, B., Lohmann, G.P., Smith, W.K., 1977. The environmental and climatic distribution of dinoflagellate cysts in modern marine sediments from regions in the North and South Atlantic Oceans and adjacent seas. *Mar. Micropaleontol.* 2, 121–200. [https://doi.org/10.1016/0377-8398\(77\)90008-1](https://doi.org/10.1016/0377-8398(77)90008-1).
- Wang, D., White, J.R., Delaune, R.D., Yu, Z., Hu, Y., 2021. Peripheral freshwater deltaic wetlands are hotspots of methane flux in the coastal zone. *Sci. Total Environ.* 775, 145784 <https://doi.org/10.1016/j.scitotenv.2021.145784>.
- Warny, S.A., Wrenn, J.H., 2002. Upper Neogene dinoflagellate cyst ecostratigraphy of the Atlantic coast of Morocco. *Micropaleontology* 48 (3), 257–272.
- Warny, S.A., Bart, P.J., Suc, J.P., 2003. Timing and progression of climatic, tectonic and glacioeustatic influences on the Messinian Salinity Crisis. *Palaeogeogr. Palaeoclimatol. Palaeoecol.* 202 (1–2), 59–66. [https://doi.org/10.1016/S0031-0182\(03\)00615-1](https://doi.org/10.1016/S0031-0182(03)00615-1).
- Wazneh, H., Gachon, P., Laprise, R., de Vernal, A., Tremblay, B., 2021. Atmospheric blocking events in the North Atlantic: trends and links to climate anomalies and teleconnections. *Clim. Dyn.* 56, 2199–2221. <https://doi.org/10.1007/s00382-020-05583-x>.
- Westerhold, T., Marwan, N., Drury, A.J., Liebrand, D., Agnini, C., Anagnostou, E., Barnett, J.S.K., Bohaty, S.M., De Vleeschouwer, D., Florindo, F., Frederichs, T., Hodell, D.A., Holbourn, A.E., Kroon, D., Lauretano, V., Littler, K., Lourens, L.J., Lyle, M., Pälike, H., Röhl, U., Tian, J., Wilkens, R.H., Wilson, P.A., Zachos, J.C., 2020. An astronomically dated record of Earth's climate and its predictability over the last 66 million years. *Science* 369 (6509), 1383–1387. <https://doi.org/10.1126/science.aba6853>.
- Xiao, F., She, Y., She, J., Zhang, J., Zhang, X., Luo, C., 2022. Assessing habitat suitability and selecting optimal habitats for relict tree *Cathaya argyrophylla* in Hunan, China: Integrating pollen size, environmental factors, and niche modeling for conservation. *Ecol. Indic.* 145, 109669 <https://doi.org/10.1016/j.ecolind.2022.109669>.
- Zachariasse, W.J., Lourens, L.J., 2022. The Messinian on Gavdos (Greece) and the status of currently used ages for the onset of the MSC and gypsum precipitation. *NewsL.* 333–360 <https://doi.org/10.1127/nos/2021/0677>.
- Zachos, J., Pagani, M., Sloan, L., Thomas, E., Billups, K., 2001. Trends, rhythms, and aberrations in global climate 65 Ma to present. *Science* 292 (5517), 686–693. <https://doi.org/10.1126/science.1059412>.
- Zonneveld, K.A.F., Pospelova, V., 2015. A determination key for modern dinoflagellate cysts. *Palynology* 39 (3), 387–409.
- Zonneveld, K.A.F., Marret, F., Versteegh, G.J., Bogus, K., Bonnet, S., Bouimetarhan, I., Crouch, E., De Vernal, A., Elshaniawany, R., Edwards, L., Esper, O., Forke, S., Grosfeld, K., Henry, M., Holzwarth, U., Kieft, J.F., Kim, S.Y., Ladouceur, S., Ledu, D., Chen, L., Limoges, A., Londeix, L., Lu, S.H., Mahmoud, M.S., Marino, G., Matsouka, K., Matthiessen, J., Mildenhall, D.C., Mudie, P.J., Neil, H.L., Pospelova, V., Qi, Y., Radi, T., Richerol, T., Rochon, A., Sangiorgi, F., Solignac, S., Turon, J.L., Verleye, T., Wang, Y., Wang, Z., Young, M., 2013. Geographic Distribution of Dinoflagellate Cysts in Surface Sediments. <https://doi.org/10.1594/PANGAEA.818280>.